AD-A192 378 PLASMOID PROPAGATION(U) MISSION RESEARCH CORP 1/1
ALBUQUERQUE NM G F KIUTTU ET AL. 12 FEB 88
MRC/ABQ-R-1039 AFOSR-TR-88-0382 F49620-85-C-0022
UNCLASSIFIED F/G 20/9 NL

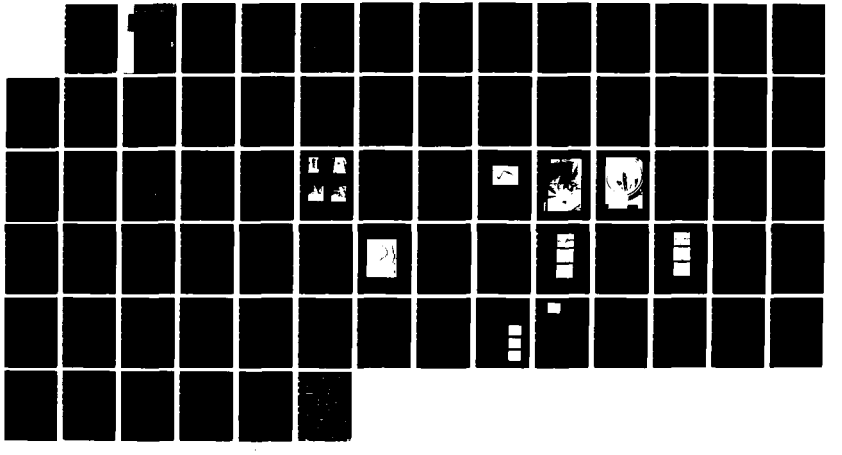

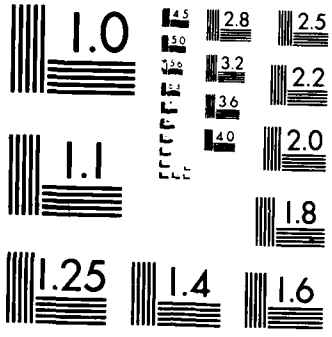
1.0
1.1
1.25
1.4
1.6
1.8
2.0
2.2
2.5
2.8
3.2
3.6
4.0
4.5
5.0

MRC/ABQ-R-1039
Copy 3

Mission Research Corporation

FINAL REPORT: PLASMOID PROPAGATION

AFOSR-TR- 88-0382

Gerald. F. Kiuttu
Richard J. Adler†
Robert J. Richter-Sand
Michael K. Williams

February 1988

Prepared for: AIR FORCE OFFICE OF SCIENTIFIC RESEARCH
Physics Directorate
Bolling Air Force Base
Washington, DC 20332

Under Contract: F49620-85-C-0022

Prepared by: MISSION RESEARCH CORPORATION
1720 Randolph Road, SE.
Albuquerque, New Mexico 87106

†NORTH STAR RESEARCH CORPORATATION
5555 Zuni, SE., Suite 345
Albuquerque, New Mexico 87108

Research sponsored by the Air Force Office of Scientific Research (AFOSR), under contract #F49620-85-C-0022. The United States Government is authorized to reproduce and distribute reprints for governmental purposes notwithstanding any copyright notation herein. This manuscript is submitted for publication with the understanding that the United States Government is authorized to reproduce and distribute reprints for government purposes.

REPORT DOCUMENTATION PAGE

1a. REPORT SECURITY CLASSIFICATION UNCLASSIFIED	1b. RESTRICTIVE MARKINGS
2a. SECURITY CLASSIFICATION AUTHORITY NA	3. DISTRIBUTION/AVAILABILITY OF REPORT Research sponsored by the Air Force Office of Scientific Research (AFOSR), under contract (Continued on reverse side)
2b. DECLASSIFICATION/DOWNGRADING SCHEDULE NA	
4. PERFORMING ORGANIZATION REPORT NUMBER(S) MRC/ABQ-R-1039	5. MONITORING ORGANIZATION REPORT NUMBER(S) AFOSR-TR- 88-0382
6a. NAME OF PERFORMING ORGANIZATION MISSION RESEARCH CORPORATION 6b. OFFICE SYMBOL (If applicable)	7a. NAME OF MONITORING ORGANIZATION Physics Directorate AIR FORCE OFFICE OF SCIENTIFIC RESEARCH
6c. ADDRESS (City, State, and ZIP Code) 1720 Randolph Road, SE. Albuquerque, New Mexico 87106	7b. ADDRESS (City, State, and ZIP Code) Bolling Air Force Base Washington, DC 20332
8a. NAME OF FUNDING/SPONSORING ORGANIZATION Same As 7a 8b. OFFICE SYMBOL (If applicable) N/A	9. PROCUREMENT INSTRUMENT IDENTIFICATION NUMBER F49620-85-C-0022
8c. ADDRESS (City, State, and ZIP Code) Same As 7b	10. SOURCE OF FUNDING NUMBERS PROGRAM ELEMENT NO: 6110?F; PROJECT NO: 8301; TASK NO: A7; WORK UNIT ACCESSION NO:
11. TITLE (Include Security Classification) PLASMOID PROPGATION	
12. PERSONAL AUTHOR(S) Kiuttu, G. F., Adler, R. J., Richter-Sand, R. J., Williams, M. K.	
13a. TYPE OF REPORT Final	13b. TIME COVERED FROM 11/84 TO 10/86
14. DATE OF REPORT (Year, Month, Day) 1988/02/12	15. PAGE COUNT 67
16. SUPPLEMENTARY NOTATION	

17. COSATI CODES		
FIELD	GROUP	SUB-GROUP

18. SUBJECT TERMS (Continue on reverse if necessary and identify by block number)
Plasmoids, Charged Particle Beams, Beam Propagation; Ion Diodes, Pulsed Power.

19. ABSTRACT (Continue on reverse if necessary and identify by block number)

Simple analytical considerations suggest that for certain parameter regimes for costreaming ion and electron beams, radial equilibrium can be expected without charge or current neutrality. To investigate these predictions experimentally, a pulsed power system comprising separate anode and cathode pulsers was designed and assembled. A double diode was developed to produce the plasmoids, and its steady-state space charge limited current properties studied analytically. Propagation of plasmoids produced in the diode has been researched over modest distances in terms of net current transport, radial profile, and beam front velocity. The results described in this report include the analysis and methodology leading to the successful production of nonneutral plasmoids and their propagation over distances up to several drift tube radii at currents more than an order of magnitude larger than predicted for either electron or ion constituents separately.

20. DISTRIBUTION/AVAILABILITY OF ABSTRACT ☐ UNCLASSIFIED/UNLIMITED ☒ SAME AS RPT ☐ DTIC USERS	21. ABSTRACT SECURITY CLASSIFICATION UNCLASSIFIED
22a. NAME OF RESPONSIBLE INDIVIDUAL Lt Col Bruce G. Smith	22b. TELEPHONE (Include Area Code) (202) 767-4908
	22c. OFFICE SYMBOL NP

DD FORM 1473, 84 MAR 83 APR edition may be used until exhausted
All other editions are obsolete

Continued from Block 3, Distribution/Availability of Report

#F49620-85-C-0022. The United States Government is authorized to reproduce and distribute reprints for governmental purposes notwithstanding any copyright notation herein. This manuscript is submitted for publication with the understanding that the United States Government is authorized to reproduce and distribute reprints for government purposes.

TABLE OF CONTENTS

LIST OF ILLUSTRATIONS

LIST OF ILLUSTRATIONS (Concluded)

I. EXECUTIVE SUMMARY

Plasmoids (Ref. 1) are ensembles of electrons and ions possessing significant directed energy in vacuum. With the development of intense ion beam technology (Ref. 2), one can realistically discuss the production of plasmoids of high kinetic energy (i.e., many megajoules) which have high velocity (~.5c). Plasmoids of this type could potentially be used in ballistic missile defense applications, since large energies are involved and target coupling is very good.

In order to assess the feasibility of plasmoid directed weapons, gaps in our knowledge of plasmoid equilibrium, stability, and propagation need to be closed. To initiate this assessment, Mission Research Corporation (MRC) performed a two-year primarily experimental investigation of non-neutral plasmoids. Nonneutral plasmoids are those which require neither charge nor current neutrality for equilibrium.

The nonexperimental part of the study included simple analytical estimates of expected parameter regimes for radial equilibrium, and one-dimensional analysis of a plasmoid compound diode, or Virtual Cathode Ion Diode (VCID). The radial equilibrium analysis made use of a simple double uniform-density, cold coaxial electron-ion beam model. Be examining the net radial electromagnetic force acting on the outermost particles, parameter regimes with differing velocities, radii, and densities were identified which satisfied the requirement for a net pinch force. These results were used to guide the design of a pulsed power system for the experiments.

To produce the plasmoids, a novel vacuum double diode consisting of a pulse-biased cold cathode and transmissive pulse-biased anode was examined analytically in terms of one-dimensional space charge limits. This analysis yielded results which predicted the possibility of current enhancements over bipolar flow, as well as single-specie, planar diodes. For certain parameters higher ion production efficiencies than obtainable

from conventional ion diodes was seen. The novel feature of this VCID is the active neutralization of the accelerated ion beam with costreaming electrons. A VCID-type diode was designed and operated for the experiments, but its capabilities were not studied extensively.

The experiments demonstrated the ability to produce plasmoids with independent pulsed power supplies for electron and ion beam constituents. One effect noted in the experiments was the non-zero turn-on time for ions. This effect is the result of the requirement for anode plasma formation prior to ion extraction, and had an adverse impact on the experiments because of the relatively short pulses available from the pulsers.

The ion delay exacerbated the problem of plasmoid propagation because of the widely disparate electron and ion velocities. Nevertheless, monitors places downstream of the diode at a distance of several drift tube radii showed evidence of current transport an order of magnitude in excess of the single-specie space charge limits. Furthermore, beam profile measurements indicated a centrally peaked current density distribution, as expected from force balance considerations.

The experimental results qualitatively substantiate the radial equilibrium analysis and lead to a relatively consistent picture of plasmoid production and propagation. The data suggest the early time formation of an electron beam well above the space charge limit of vacuum propagation. As the anode plasma forms and ions become available for acceleration, both species enter the drift tube where faster electrons continuously emerge through the ion beam front and diverge radially due to the local space charge. The plasmoid then propagates at the ion velocity as long as electron current can be supplied.

Unfortunately, due to the short electrical pulse lengths, the plasmoids could not be propagated more than a fraction of a meter, thus precluding the determination of long-distance stability and magnetic cross-field propagation characteristics.

II. THEORY

1. INTRODUCTION

A nonneutral plasmoid is a ion-electron plasma with net directed energy and neither charge, nor current neutral. On the basis of a straightforward analysis, equilibrium is expected for certain parameter regimes of electron and ion velocities and current ratios. To generate this type of plasmoid, individual control of ion and electron species is required. In previous ion diode and collective ion acceleration schemes, either no direct attempt at neutralization was made, or the neutralizing particles were generated without net drift energy (Refs. 3, 4, 5, and 6). MRC's approach to ion and electron production is illustrated in Figure 1.

2. RADIAL EQUILIBRIUM

Charged particle beams propagating in pinched equilibrium usually assume a Bennett-like current density profile (Ref. 7), $j(r) \sim (1+r^2/a^2)^{-2}$, where the Bennett radius, 'a', is related to the transverse particle energy or beam temperature. To simplify our initial analysis, we assumed uniform beam profiles, with uniform axial velocity fields and no transverse energy (cold beam limit). The radii of the two collinear species are r_e and r_i for the electrons and ions, respectively, as shown in Figure 2.

In the one-dimensional analysis, we examined the net radial forces acting on the outermost particles (since they are the least confined). The other quantities of interest are total currents, I_e and I_i, and axial velocities, v_e and v_i. The net radial force acting on the particles is given by the Lorentz force,

$$F_{e,i} = \mp e \left(E_r - v_{e,i} B_\theta\right) \quad , \tag{1}$$

where the minus sign corresponds to the electrons.

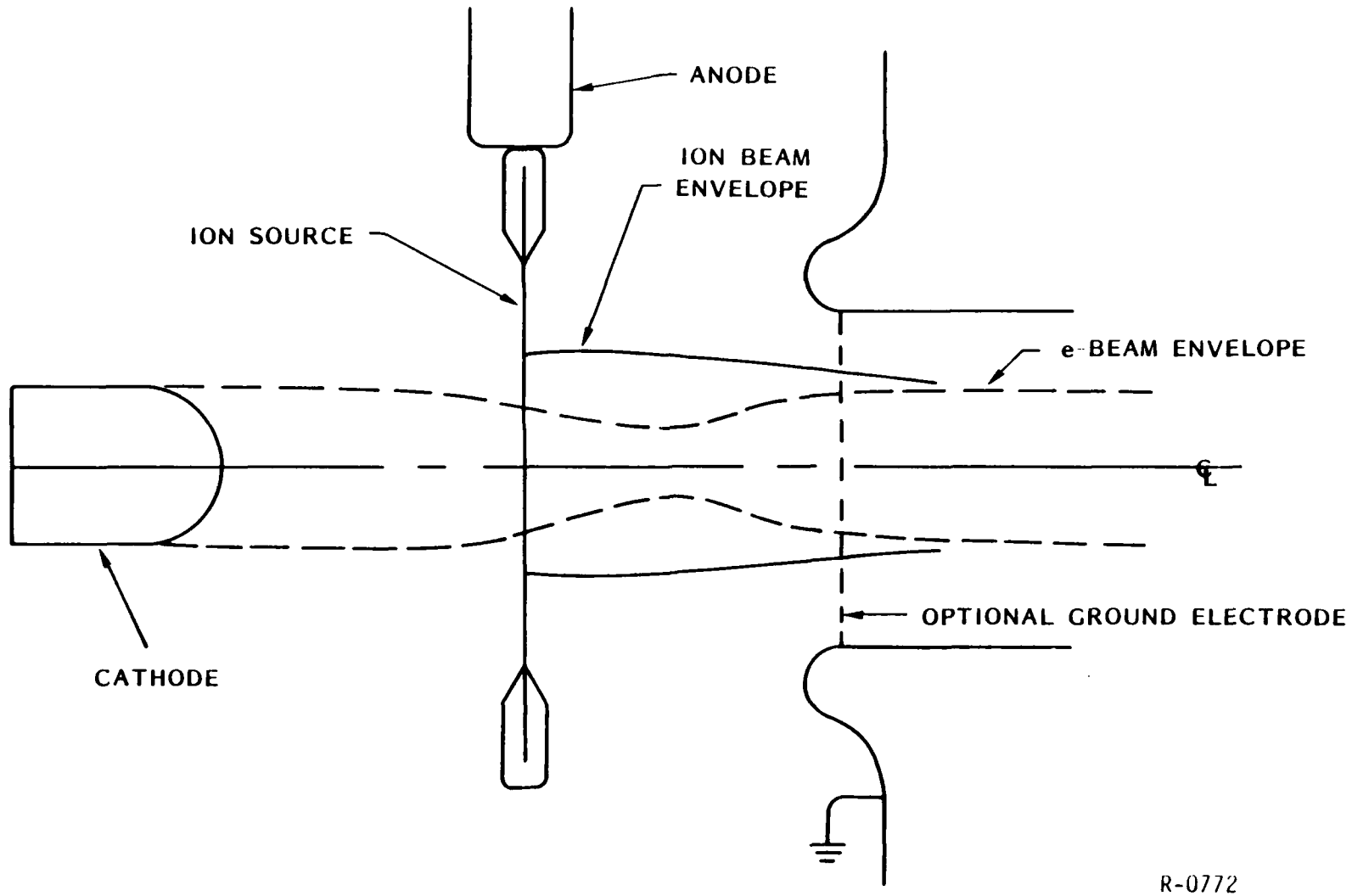

Figure 1. Schematic of the diode geometry for plasmoid formation.

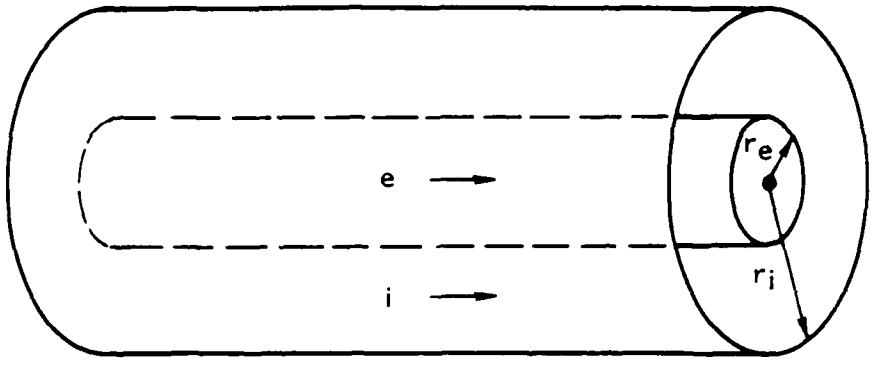

R-0772

Figure 2. A rectangular profile electron beam of radius r_e propagating concentrically with an ion beam of radius r_i.

For plasmoid radial equilibrium, the net force must be negative (that is, a pinch force). If we define the dimensionless quantities $\eta = (r_e/r_i)^2$ $f = -I_i/I_e > 0$, and $\nu = v_i/v_e$, then radial confinement of electrons at r_e requires

$$\eta f \geq \frac{\nu(1-\beta_e^2)}{(1-\nu\beta_e^2)} \qquad \text{for } \eta \leq 1 \tag{2}$$

$$f > \frac{\nu(1-\beta_e^2)}{(1-\nu\beta_e^2)} \qquad \text{for } \eta \geq 1 \tag{3}$$

where β_e is the usual v_e/c.

For the ions at r_i, we find

$$f \leq \frac{\nu(1-\beta_e^2)}{(1-\nu^2\beta_e^2)} \qquad \text{for } \eta \leq 1 \tag{4}$$

$$\eta f \leq \frac{\nu(1-\beta_e^2)}{(1-\nu^2\beta_e^2)} \qquad \text{for } \eta \geq 1 \tag{5}$$

The various inequalities were combined to yield the following relations:

$$\frac{\beta_i}{\beta_e}\,\frac{(1-\beta_e^2)}{(1-\beta_i\beta_e)} \leq \eta f \leq \frac{\beta_i}{\beta_e}\,\frac{(1-\beta_i\beta_e)}{(1-\beta_i^2)} \tag{6}$$

$$\frac{\beta_i}{\beta_e}\,\frac{(1-\beta_e^2)}{(1-\beta_i\beta_e)} \leq f \leq \frac{\beta_i}{\beta_e}\,\frac{(1-\beta_i\beta_e)}{(1-\beta_i^2)} \tag{7}$$

$$\frac{(1-\beta_e^2)\,(1-\beta_i^2)}{(1-\beta_i\beta_e)^2} \leq n \leq \frac{(1-\beta_i\beta_e)^2}{(1-\beta_i^2)\,(1-\beta_e^2)} \tag{8}$$

For a characteristic area ratio of $n = 1$ (equivalent electron and ion radii), we obtain a geometric mean value for f of

$$\langle f \rangle = \frac{\beta_i \gamma_i}{\beta_e \gamma_e} \tag{9}$$

where γ_i, γ_e are species relativistic factors.

The equilibrium expected for electron velocities of .5c and .9c is graphed schematically in Figures 3 and 4. The beam area ratio for equilibrium is shown in Figures 5 and 6. The relative size of the area in parameter space corresponding to equilibrium increases as the electron energy increases. We were able to define an equilibrium figure of merit, $(f_{max}-f_{min})/\nu$, as a quantitative measure of this area and is grapned in Figure 7.

In reality, the areas corresponding to equilibrium are reduced since the radial pressure force due to the non-zero transverse particle energy was neglected in our derivations. A more exact equilibrium analysis would have included temperature effects. Still another constraint on radial equilibrium parameters is space charge. Each particle's potential energy (charge times potential) cannot exceed its initial energy, or energy conservation would be violated. The above analysis served as a useful guide to investigate radial equilibrium conditions.

3. VIRTUAL CATHODE ION DIODE

The Virtual Cathode Ion Diode (VCID) was conceived as the means of producing nonneutral plasmoids. It is shown conceptually in Figure 8. The diode operates on the following principles. An electron beam is injected

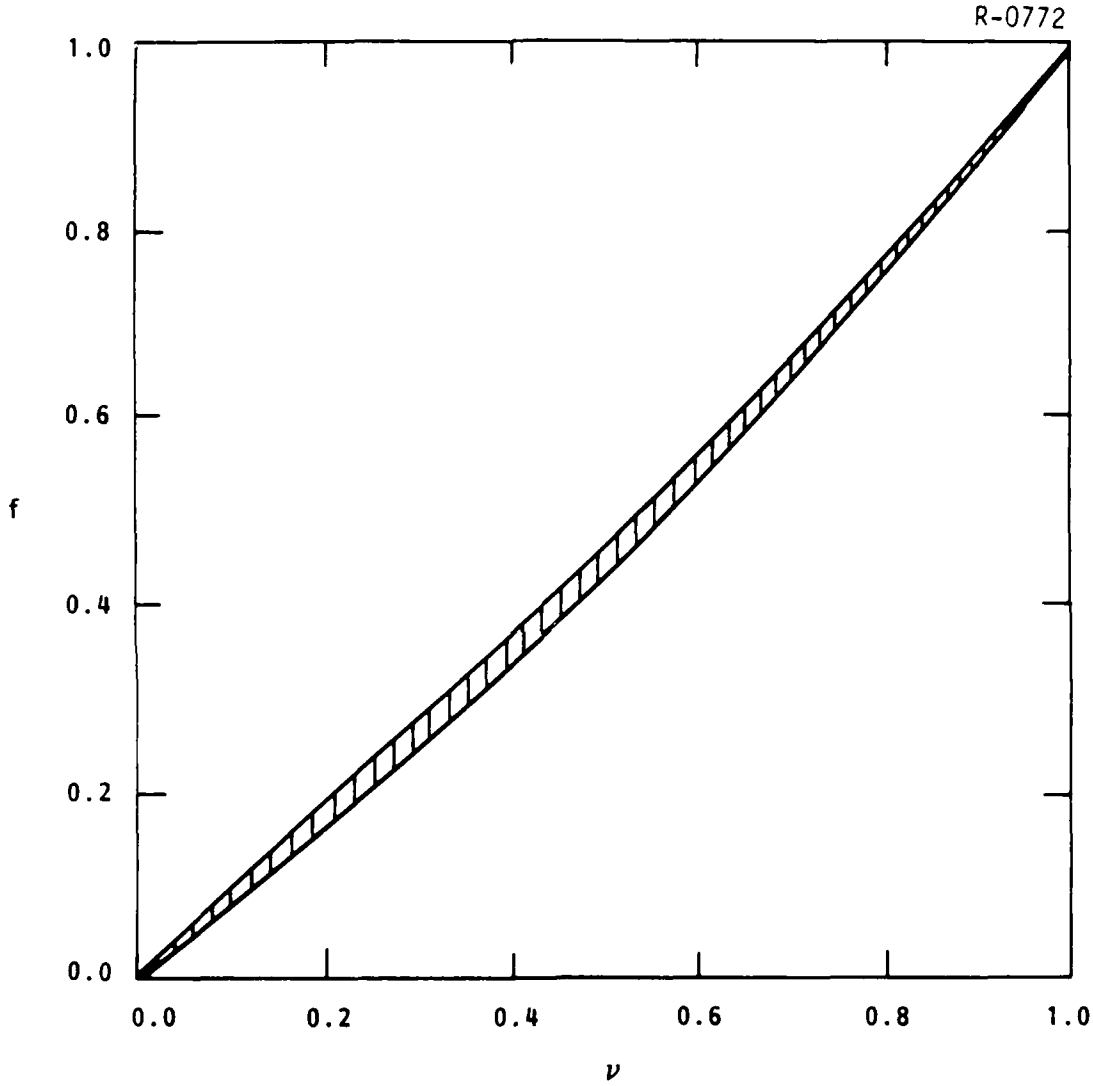

Figure 3. Range of equilibria (shaded area) in (ν,f) space for β_e = 0.5.

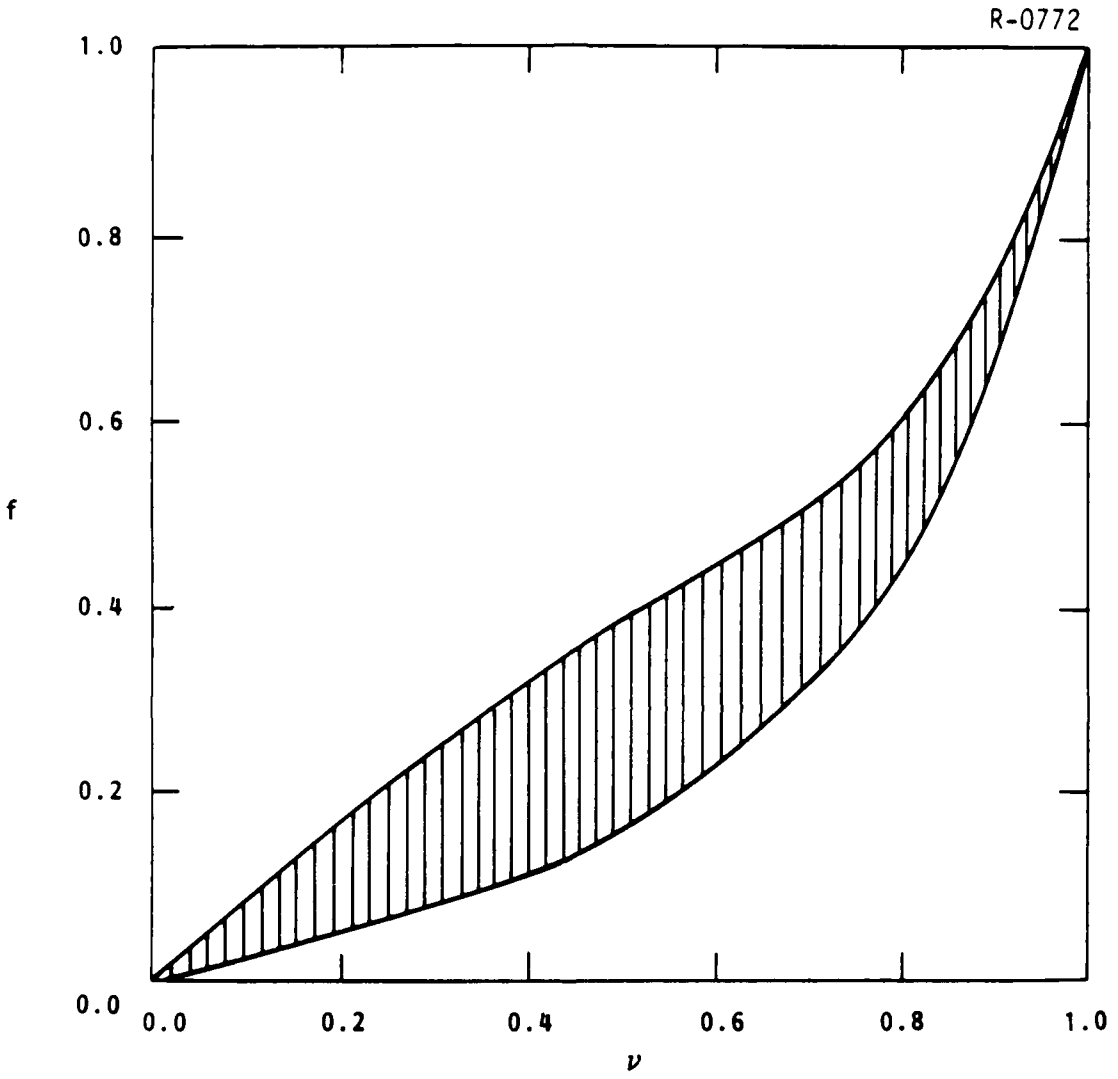

Figure 4. Range of equilibria (shaded area) in (ν,f) space for β_e = 0.9.

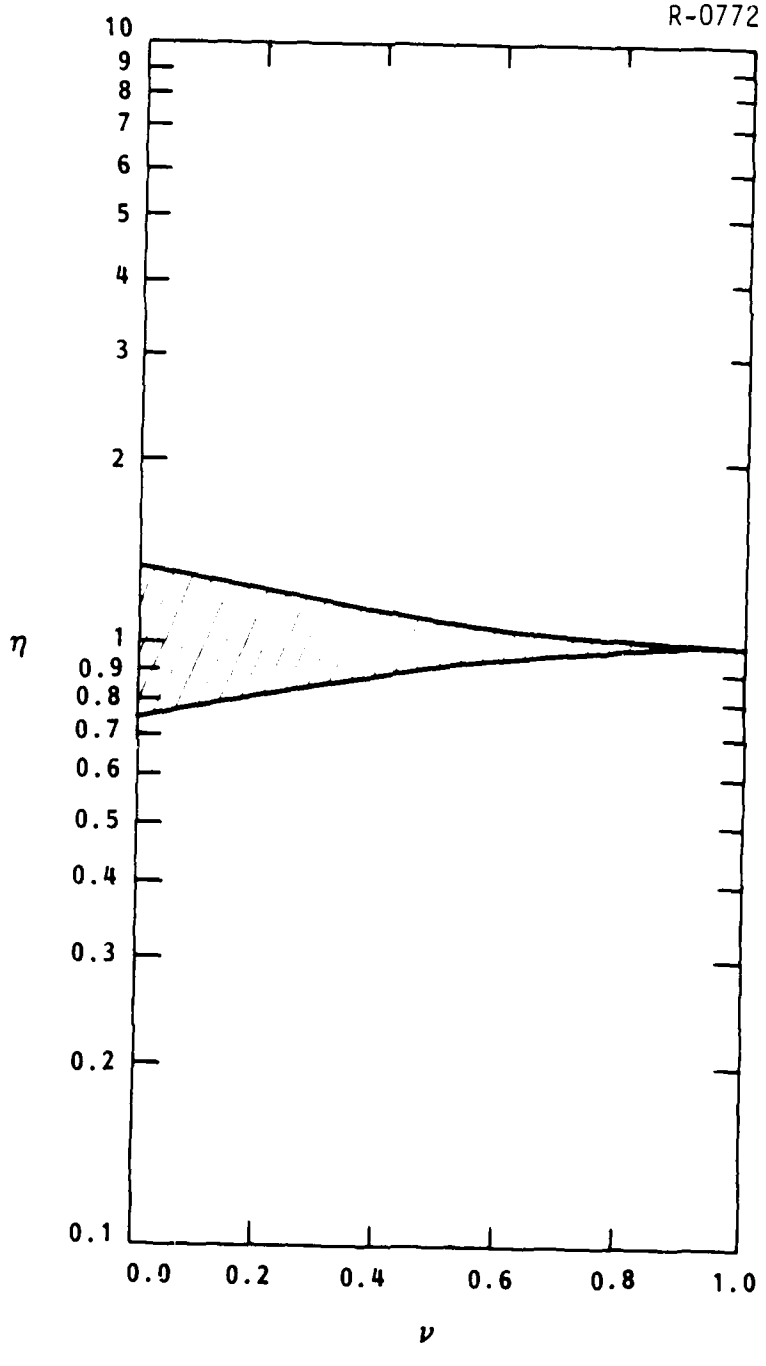

Figure 5. Range of equilibria (shaded area) in (ν,n) space for β_e = 0.5.

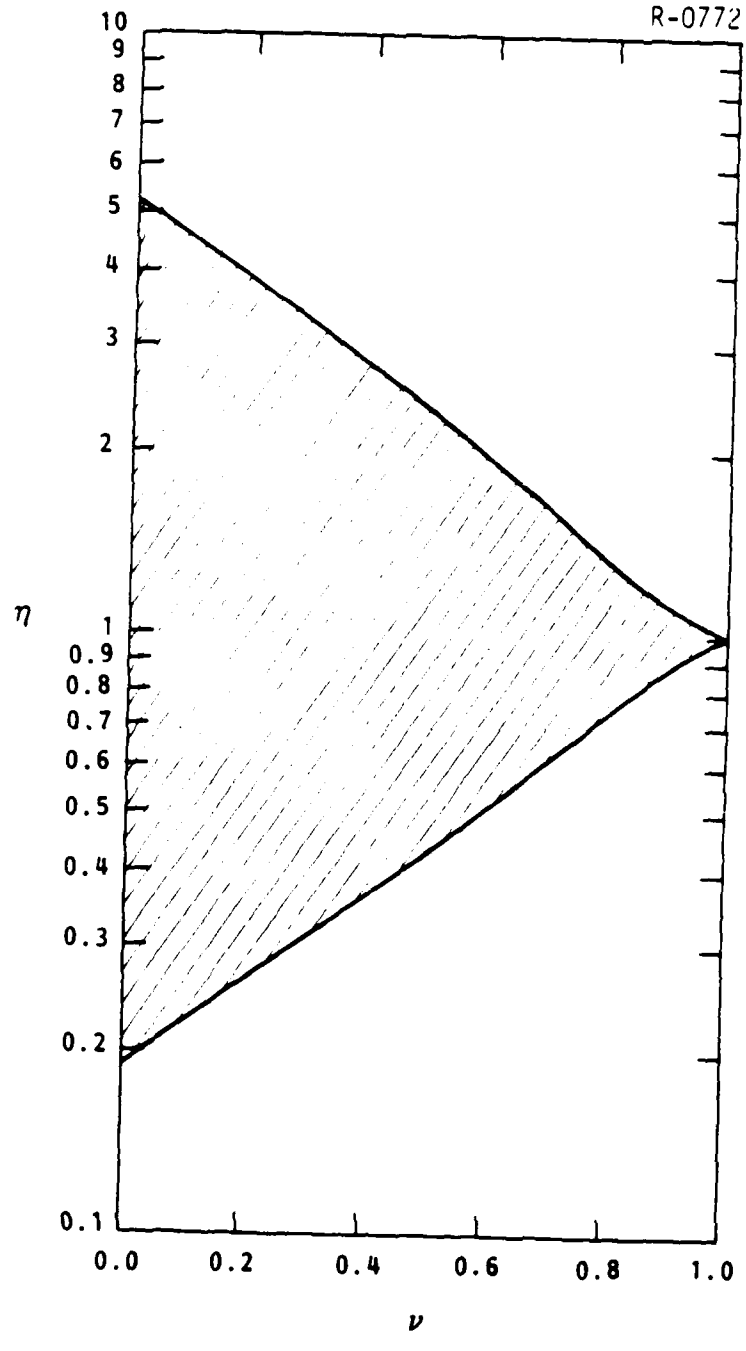

Figure 6. Range of equilibria (shaded area) in (ν,η) space for β_e = 0.9.

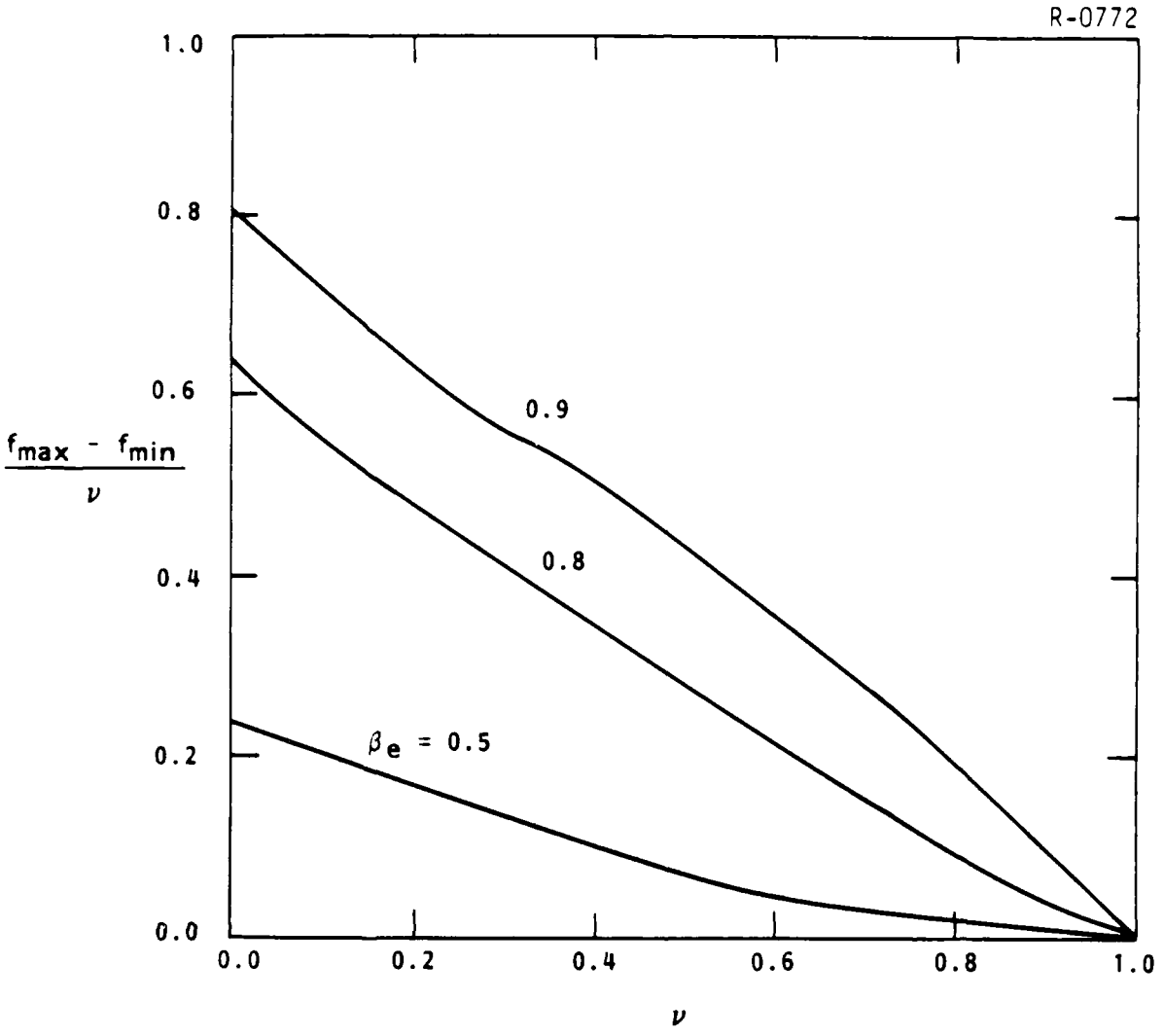

Figure 7. Equilibrium sensitivity figure of merit for three values of β_e.

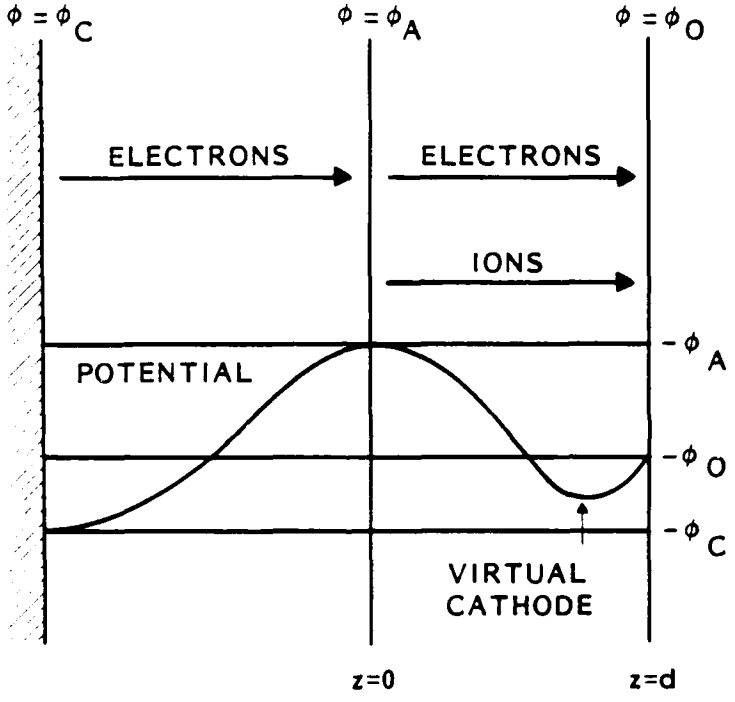

Figure 8. The virtual cathode ion diode.

into an ion acceleration gap with sufficient energy to completely traverse it and emerge at the other side. The presence of the comoving electrons within the ion gap provides space charge neutralization of the ions and increases the achievable current density. If sufficient electrons are injected, the diode potential actually swings negative. This potential reversal has the beneficial effect of inhibiting electron emission and backflow from the grounded electrode, resulting in very high ion power efficiencies. Since the electrons emerge travelling in the same direction as the accelerated ions, they are available for charge and current neutralization in the drift region, again increasing the limiting current densities.

The VCID was analyzed using a one-dimensional, two-species, steady-state, nonrelativistic planar formalism (Ref. 8). The following nonlinear ordinary differential equation describes the potential in the gap ($o \leq z \leq d$)

$$\frac{d^2\phi}{dz^2} = -\frac{1}{\varepsilon_o}\left[j_i\left(\frac{m_i}{2Ze}\right)^{1/2}(\phi_A-\phi)^{-1/2} - j_e\left(\frac{m_e}{2e}\right)^{1/2}(\phi-\phi_C)^{-1/2}\right], \quad (10)$$

where ϕ_C is the cathode potential, ϕ_A the anode potential, Z is the ion charge, and $m_e(m_i)$ and $j_e(j_i)$ are the electron (ion) mass and current density. The boundary conditions for the problem are the fixed electrode potentials and space charge limited ion flow ($d\phi/dz = 0$) at the anode.

The differential equation was solved by a combination of analytical and numerical methods. It was found that solutions exist only for j_i, j_e, and ϕ_C lying on a particular surface in the three-dimensional parameter space. If we define the normalized (to the single species Child-Langmuir space charge limiting) current densities

$$J_i = \frac{j_i}{j_i^{CL}} = \frac{9}{4}\left(\frac{m_i}{2Ze}\right)^{1/2}\frac{j_i d^2}{\varepsilon_o(\phi_A-\phi_O)^{3/2}} \quad (11)$$

and

$$J_e = \frac{j_e}{j_e^{CL}} = \frac{9}{4}\left(\frac{m_e}{2Ze}\right)^{1/2} \frac{j_e d^2}{\varepsilon_o(\phi_A-\phi_0)} \tag{12}$$

and the normalized electron potential

$$p = \frac{(\phi_A-\phi_C)}{(\phi_A-\phi_0)} \tag{13}$$

then a slice of the parameter solution in the p = 1.1 plane looks like the curve in Figure 9. Point C is the generalized 'bipolar flow' (Ref. 9) case ($d\phi/dz = 0$ at the downstream electrode). For this special case, the relationship between the normalized current densities is

$$J_i = J_e\left[p^{1/2} - (p-1)^{1/2}\right] \quad . \tag{14}$$

For higher current densities along the solution curve (C to E), the normalized potential, $y = (\phi_A-\phi)/(\phi_A-\phi_0)$, actually exceeds unity (that is, a negative potential barrier forms) within the gap. As one proceeds along the curve from point C, the potential barrier rises monotonically, until E, where the potential barrier equals the incident electron energy. It is in the region between points C and E where the VCID operates.

If we take as a minimum operating point for the VCID, point C, then we can plot J_i (for protons) and J_e as a function of electron energy, as in Figure 10. The important point brought out by Figure 10 is that for modest variation in relative electron energy, ion current densities can be enhanced up to a factor of 4 over the single species limit.

4. SPACE CHARGE LIMITING CURRENTS

Evidence of plasmoid propagation is signaled by a net current in excess of the single species (unneutralized) space charge limit. Therefore, consider a beam of electrons or ions of radius r_b, propagating on

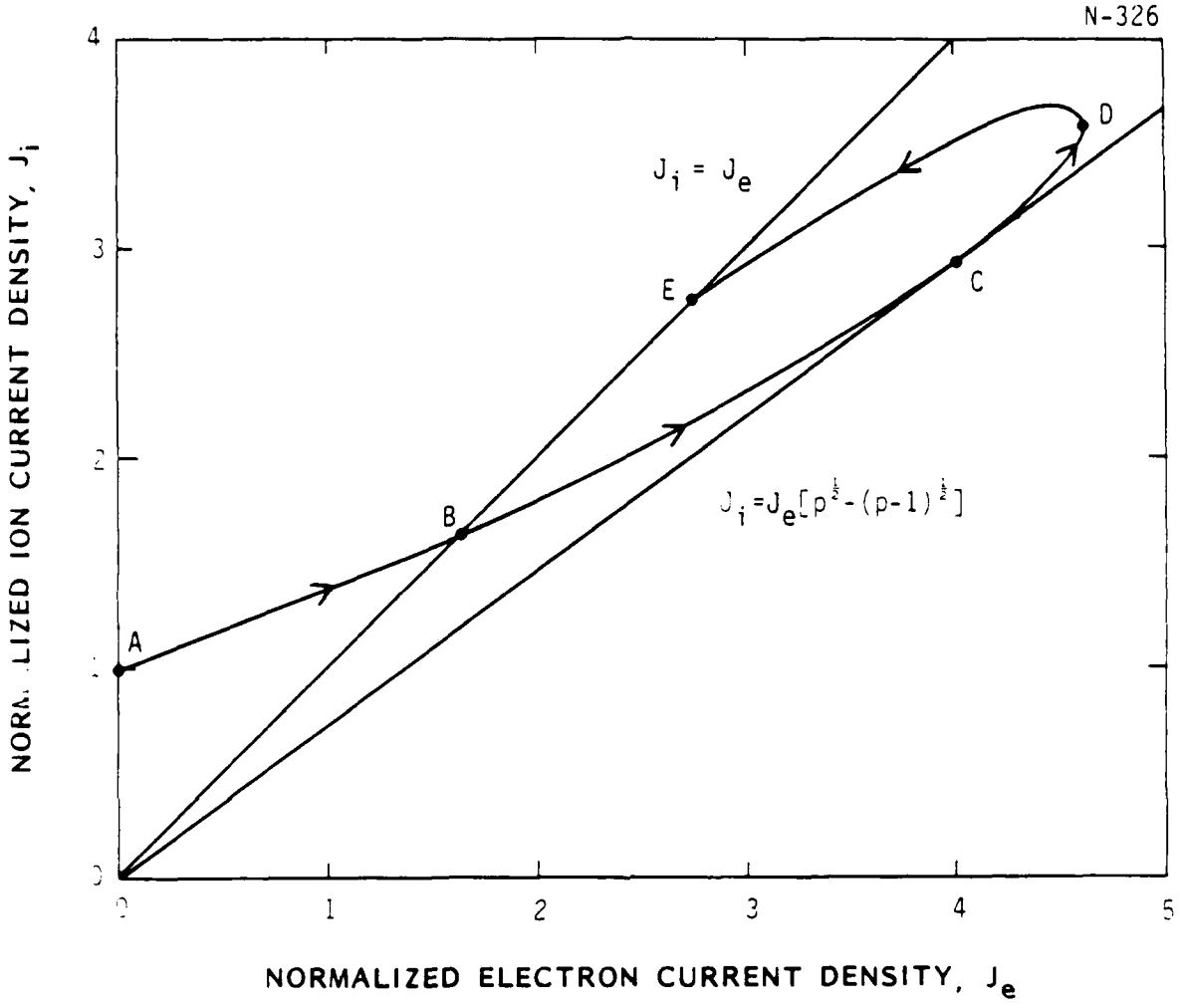

Figure 9 . Solution curve in (J_i, J_e, p) parameter space for p = 1.1.

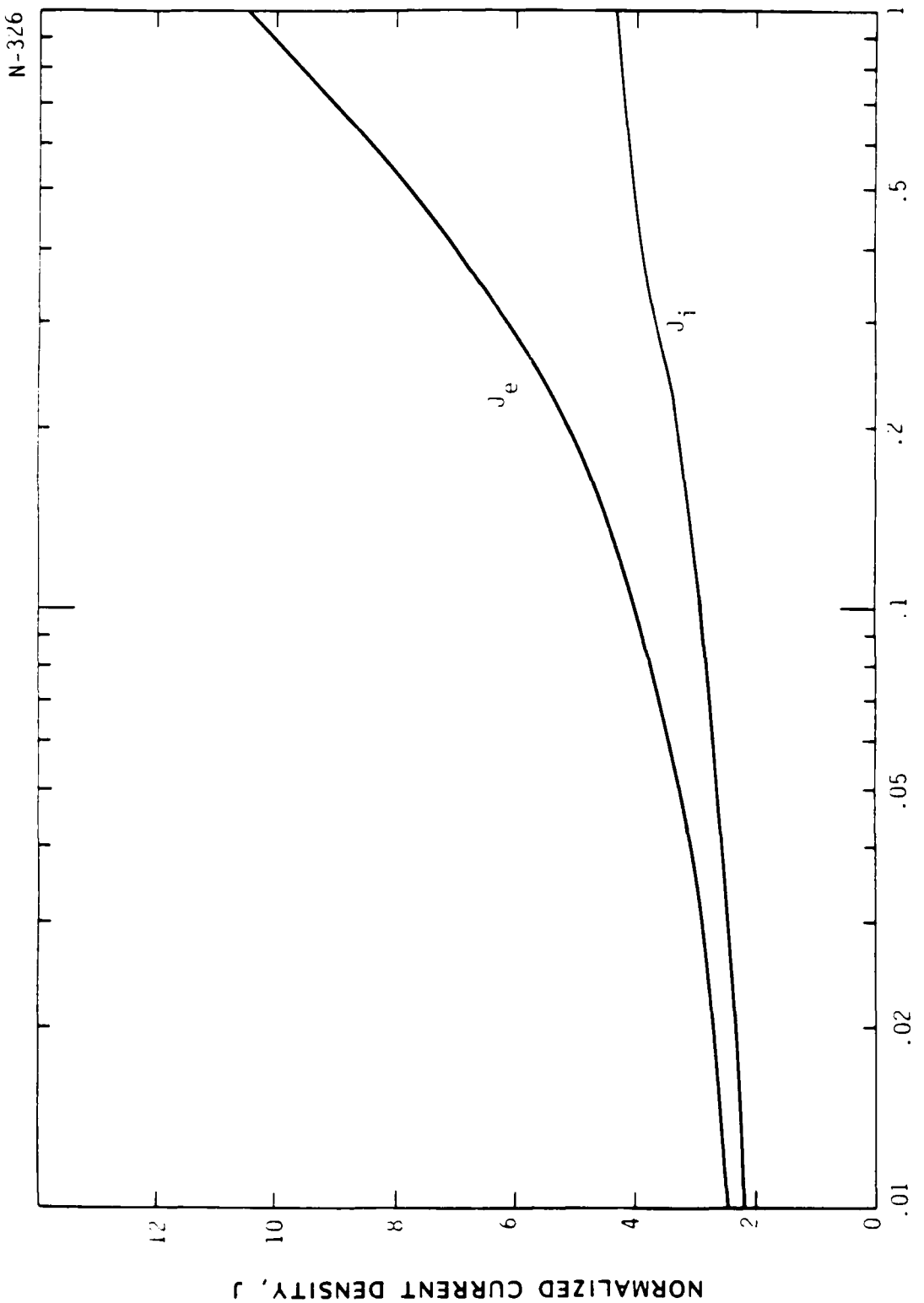

Figure 10. Ion and electron current densities at the $J_i = J_e [p^{1/2}-(p-1)^{1/2}]$ operating point.

axis within a perfect conductor of radius r_w. The space charge limiting current for this configuration is computed by evaluating the radial profile of the potential (using Poisson's equation and the continuity equation), and finding the maximum value (on axis). To make the calculation tractable, one assumes that the beam has a uniform current density and velocity distribution. In this case, using conservation of energy,

$$q\phi + \gamma\, mc^2 = \gamma_o\, mc^2 \tag{15}$$

where q, m, and $(\gamma_o - 1)\, mc^2$ are the particle charge, mass, and injected kinetic energy, one obtains

$$I(\gamma) = \frac{4\pi mc\beta\,(\gamma_o - \gamma)}{\mu_o q\left(1 + 2\,\ln\frac{r_w}{r_b}\right)} \tag{16}$$

The current is now maximized by taking the derivative with respect to γ and equating to zero to solve for γ corresponding to $I_{max} = I_L$. It is found that $\gamma = \gamma_o^{1/3}$. Upon substitution into Equation (16), we arrive at the expression

$$I_L = \frac{4\pi mc}{\mu_o q\left(1 + 2\,\ln\frac{r_w}{r_b}\right)}\quad (\gamma_o^{2/3} - 1)^{3/2} \tag{17}$$

originally published by Bogdankevich and Rukhadze (Ref. 10) for uniform beams in strong magnetic fields. Extending the result to include the effects of space charge neutralization yields:

$$I_L = \frac{17\,(\gamma_o^{2/3} - 1)^{3/2}}{(1-f_e)\,\left(1 + 2\,\ln\frac{r_w}{r_b}\right)}\quad \text{kA} \tag{18}$$

where $f_e = n_i/n_e = -I_i v_e/I_e v_i$ for electrons. The limiting electron and proton currents are plotted in Figures 11 and 12, over applicable energy ranges and for several beam-to-wall radius ratios.

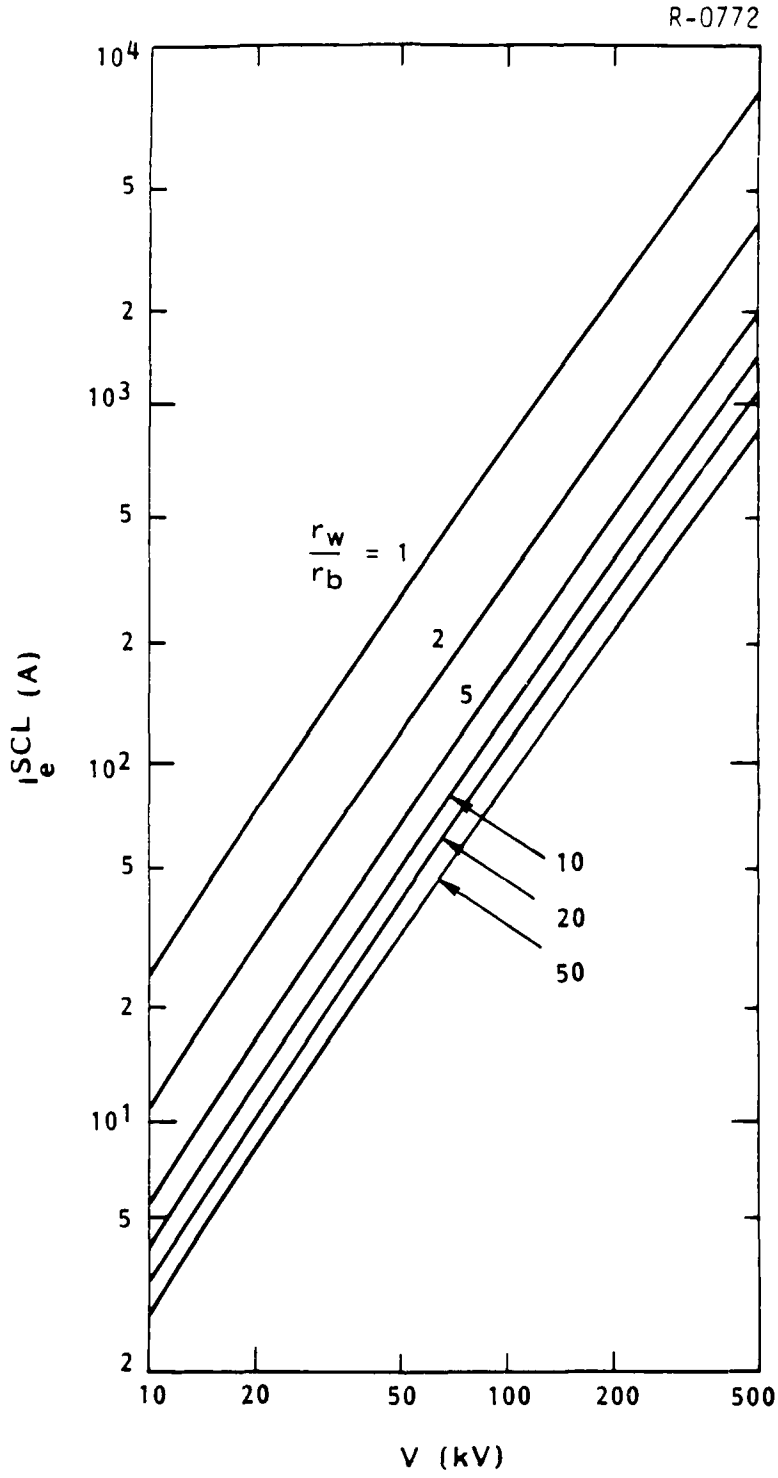

Figure 11. Normalized space charge limited electron current for various beam-to-wall radius ratios.

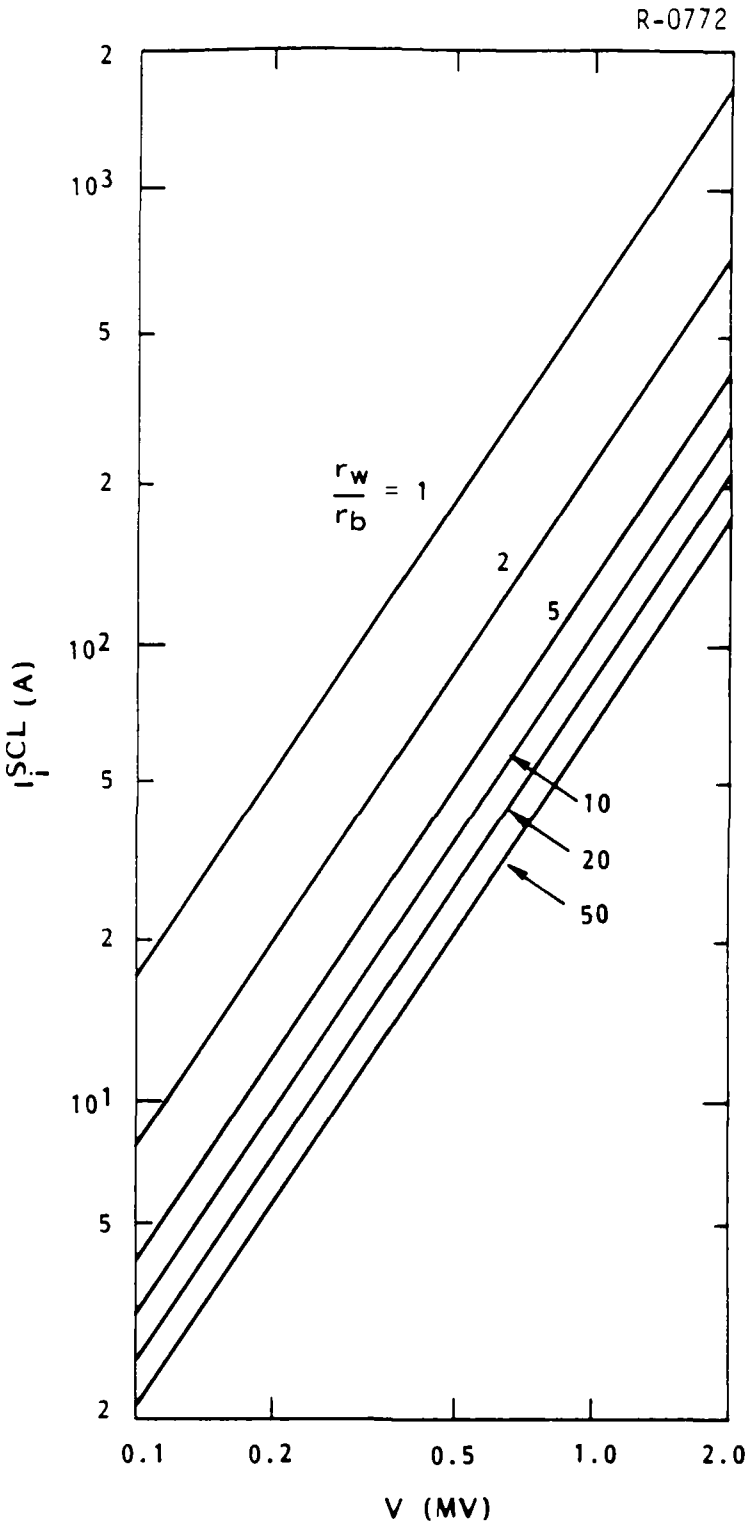

Figure 12. Normalized space charge limited ion current for various beam-to-wall radius ratios.

III. EXPERIMENT

1. CONFIGURATION

The layout of the hardware for the plasmoid generation and propagation experiments is illustrated in Figure 13. There are four major components; IMV accelerator, cathode pulser, plasmoid pulser, and screen room.

The first major piece of equipment is the Pulserad-112A accelerator built by Physics International. This Marx generator/oil Blumlein line was modified for the plasmoid experiments in the following manner. First, the normally negative output polarity was reversed to bias the anode with a positive voltage. Next, the pulseline was changed to a simple coaxial line by shorting the inner and intermediate cylindrical lines. This was done to drop the impedance and the maximum output voltage, since extremely high voltages were not necessary for these experiments. Thus, the output parameters for the accelerator were 1.6 MV maximum open circuit voltage, 20Ω line impedance, and a 30 nsec pulse length into a matched (20Ω) load. However, we routinely charged the Marx generator to only 65 percent of maximum for an open circuit output voltage of approximately 1 MV. The 112A was attached to the plamoid diode vacuum chamber via an adaptor flange which supported a diffusion pump and contained a B-dot current probe. A resistive voltage monitor was mounted at the Blumlein output.

To pulse bias the cathode independent of the anode, a transformer pulser was designed and built. The cathode pulser is rather novel in that it uses a spiral air core high voltage transformer and a low impedance solid dielectric pulseline made of special cable. A schematic diagram of the line charging circuit is shown in Figure 14. Basically, a trigger pulse is fed to a triggered spark gap switch, which completes a discharge circuit for two 1.8 μf, 50 kV capacitors through a single turn primary winding of the transformer. The transformer secondary consists of twelve

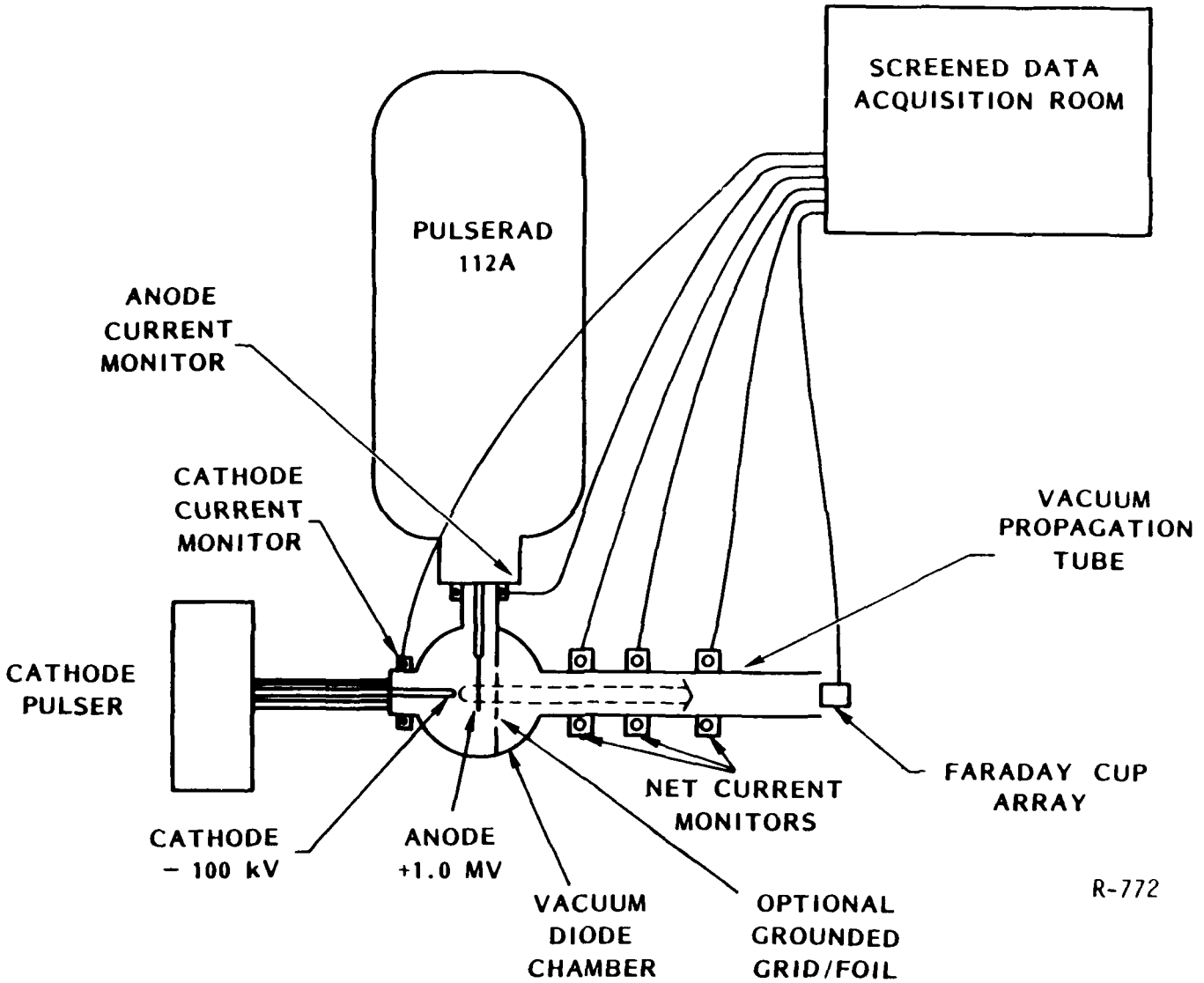

Figure 13. Plasmoid propagation experimental layout.

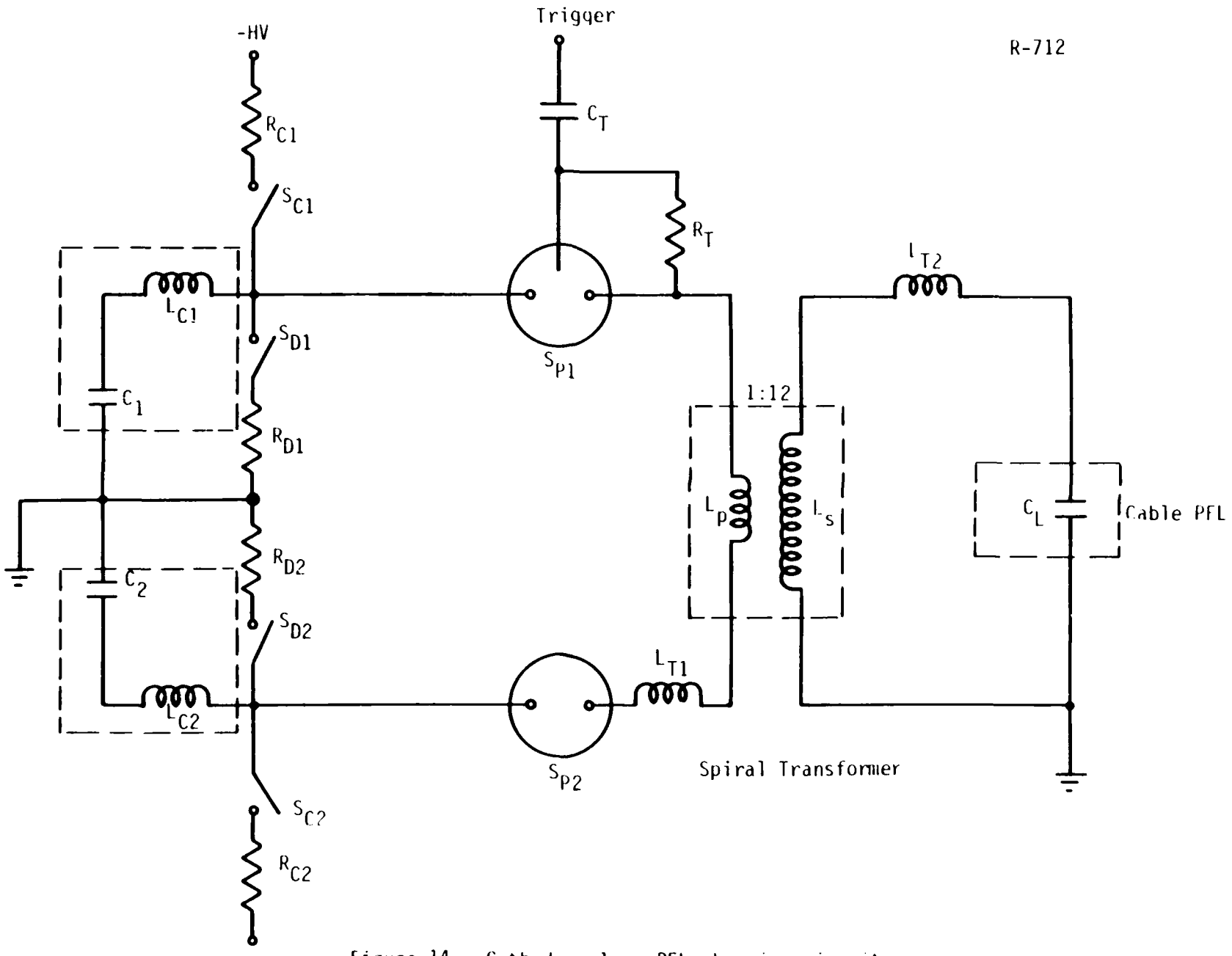

Figure 14. Cathode pulser PFL charging circuit.

turns wound concentrically within the primary. The brass foil conductorwas insulated with mylar sheet. The transformer output was fed to the cable pulseline, which acts as a lumped capacitance on the charging time scale.

The pulser was originally designed to operate near the dual resonance point to maximize energy transfer efficiency. That is, the resonant frequencies of the primary and secondary circuits are matched by tuning inductors in each circuit. Under matched conditions, the output voltage as a function of time is given by

$$V(t) = \frac{V_o}{2}\sqrt{\frac{L_2}{L_1}}\, e^{-t/T}\left[\cos\frac{\omega t}{\sqrt{1-k}} - \cos\frac{\omega t}{\sqrt{1+k}}\right], \qquad (19)$$

where $T = 4(1-k^2)L_1L_2/(R_2L_1+R_1L_2)$ and is the damping time constant. When the inductances are adjusted so the overall coupling coefficient $k = M/\sqrt{L_1L_2}$, is 0.6, then maximum secondary voltage is developed not on the first, but on the second, or reverse polarity, half cycle. Transformers of this type have recently been designed to operate at up to 1.5 MV output with better than 90 percent efficiency.

A unique feature of the MRC cathode pulser was the use of high voltage cable for a pulse forming line. Belden 8871 cable makes use of a semi-conducting polyethylene sleeve around the inner conductor of a coaxial line to reduce the maximum field stress and improve high voltage standoff to hundreds of kilovolts (pulsed) while keeping size below <1 inch in diameter. The impedance of the cable is nominally 50Ω. To reduce the line impedance further, twelve 17 foot long cables were connected in parallel, yielding an effective line impedance of about 4Ω and a pulse length of 50 nsec into a matched (4Ω) load. Photographs of the pulser are shown in Figure 15. A summary of design parameters are shown in Table 1.

VG-0534

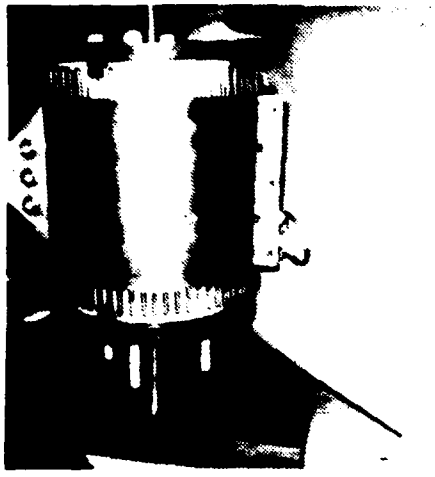

a) 12:1 SPIRAL AIR CORE TRANSFORMER

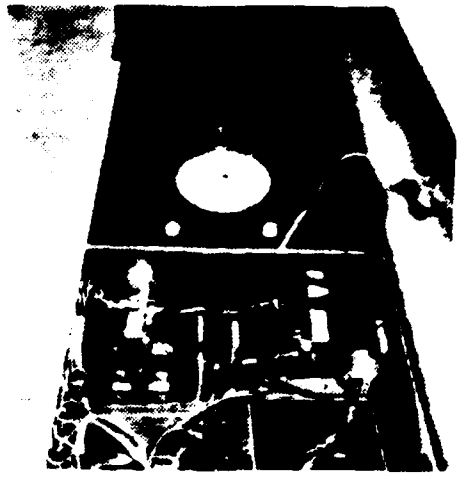

b) PULSER TANK SHOWING CHARGE, DUMP, & TRIGGER ELECTRONICS. HIGH VOLTAGE OUTPUT IS FROM ALUMINUM DISC ABOVE TRANSFORMER IN BACKGROUND.

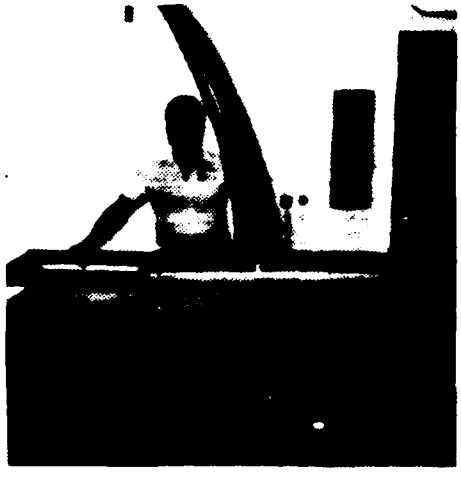

c) PULSER TANK MEASURES 46"x 18"x 36". TWO 3 kJ PRIMARY STORAGE CAPACITORS MOUNT EXTERNALLY

d) REMOTE PULSER CONTROL PANEL

Figure 15. Plasmoid cathode pulser.

TABLE I. CATHODE PULSER DESIGN SPECIFICATIONS

Output Voltage (open circuit)	$\geq$ 300 kV
Output Current (short circuit)	$\geq$ 60 kA
Output Impedance	$\leq$ 5 Ω
Peak Power (matched load)	$\geq$ 4.5 GW
Pulse Length (matched load)	48 nsec
Bank Capacitance	.9 μf
Transformer Step-up Ratio	12:1
Maximum Charge Voltage (one capacitor)	50 kV
Pulse Forming Line	12×17' Belden 8871 Cables in Parallel.
PFL Capacitance	7.2 nf
Output Switch	Dielectric Surface Flashover
Pulser Tank Size (PFL, capacitors external)	18"×36"×46"
Insulating Mediumn	Oil
Capacity	110 gal.

The output of the pulser cable pulseline shown in Figure 16 was fed to the cathode in the plasmoid diode via an oil-filled conducting elbow. A PVC insulating disc provided the interface between the oil and diode vacuum. During operation of the pulser it was discovered that, althougn the PVC insulator was designed to hold off more than the maximum cathode voltage, it failed regularly. After much testing, we concluded that the insulator suffered from reduced holdoff due to the reversal in voltage polarity and decided to operate near the peak of the first half cycle (with reversed polarity). This alleviated the breakdown problem, but caused us to operate at cathode voltages lower than planned. Nevertheless, the pulser performed well, and has proven to be a reliable, compact high voltage generator.

The third crucial component in the experimental setup is the plasmoid diode illustrated schematically in Figure 1. In this region, voltages of hundreds of kilovolts and durations of only tens of nanoseconds from the two pulsers had to be applied simultaneously to insure proper operation. This was achieved by inserting a dielectric surface flashover switch in the cathode stalk just before the tip. The materials used for the switch were PVC and lucite. The geometry was chosen so that when the cathode pulser fired, the switch would hold off the maximum pulser voltage, but break down rapidly when the capacitively coupled anode voltage was applied. Photographs of the diode vessel external and internal configurations are shown in Figures 17 and 18.

An anode which would provide a copious source of protons, and yet be extremely transmissive to the electrons streaming through from the cathode had to be designed. Experimentation with several materials and setups produced a workable design, using nylon stocking hose stretched tightly over a knitting hoop.

Finally a screen room, located far from the experiment provided a noise free environment for data acquistion. The screen room housed six Tektronix 7844 dual beam oscilloscopes and one Tektronix 7104 fast oscilloscope, for a total of 13 data recording channels. The signal cables

R-712

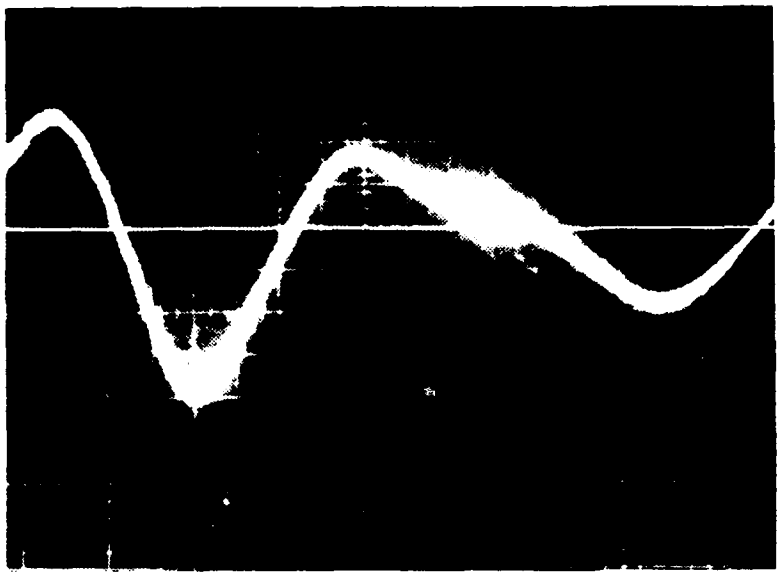

t (μsec)

Figure 16. Measured output waveform, 1 μs/cm.

Figure 17. Diode vacuum vessel configuration.

Figure 18. Plasmoid diode.

running between the screen room and experiment were solid shield UT-141 coaxial cables (50Ω) located in cable troughs below the floor. The cable lengths were measured using a time domain reflectometer (TDR) for accurate relative timing information.

2. DIAGNOSTICS

Several diagnostics were used in the course of the experiments to determine the characteristics of plasmoid formation and propagation. These included resistive voltage monitors, B-dot and Rogowski coil current monitors, an apertured Faraday cup array for net current density profile measurements, a simple magnetic particle spectrometer for determining separate ion and electron current densities on axis, and a compact Thomson parabola spectrometer. We also attempted to field CR-39 ion track detectors and time-resolved (<5 nsec) optical cameras in conjunction with NE102 fast plastic scintillator, but with limited success.

The voltage of the 112A accelerator was routinely monitored with a resistive voltage monitor located at the Blumlein output at the entrance to the diode. The inductance between the monitor and the anode is estimated to be 50 - 100 nH, so that inductive corrections to the voltage due to the L(dI/dt) drop are insignificant except for very early (t<5 nsec) in the pulse. The anode current was measured with a self-integrating B-dot loop mounted within the transition section between the machine and the vacuum diode vessel. We were able to infer the cathode voltage from measurements of the cathode pulseline voltage, anode voltage, and diode current, and assumed a resistive voltage division between the diode impedance and the 4Ω cathode pulseline impedance. The cathode current was monitored with a wall-mounted B-dot loop in the feed region. The peak current measured by the cathode and anode probes generally agreed to within about 10 percent, but the details of the time history (especially rise time) often differed significantly.

The diagnostic configuration in the plasmoid drift region is shown in Figure 19. The plasmoid net current was measured with a wall-mounted 3-dot probe 20 cm downstream from the anode within the 15 cm diameter drift of tube. For some shots, Rogowski coils were placed at several axial distances within the larger 20 cm diameter sections of drift tube. However, these monitors proved to be too sensitive to the RF noise levels present and were not quantitative useful. To determine the net (essentially electron) current density radial profiles a linear array of apertured Faraday cups, shown in Figure 20, was used. The individual apertures were 2.8 mm in diameter, and were spaced 1.71 cm apart across the diameter of the graphite housing. These detectors allowed time-resolved determination of the radial profile of the plasmoids, and a quantitative indication of radial coherence.

A simple magnetic spectrometer was constructed, as shown in Figure 21, to estimate the relative ion and electron current densities on axis. The magnetic field within the gap was approximately 800 Gauss. For the electron and ion velocities characteristic to our experiments, this field resulted in deflection of essentially all the incident electrons into the wall collectors, while allowing passage of the ions. These ions impinged on the terminal electrode. As with all detectors of this type, interpretation of the signals is complicated by the generation of secondary electrons. We estimate the secondary electron coefficient to be in the range of a few to ten. To observe the ion signature we routinely biased the ion detector with a negative voltage of about 30 V. With this voltage, the ion current is probably multiplied by a factor of 5 - 10 due to the repulsion of the secondary electrons.

To measure the voltage on the cathode, we designed and built a variation of the standard resistive divider monitor, as shown in Figure 22. In this variation, the ground side resistor is coaxial rather than planar (axial), with a resistance given by

$$R = \frac{\rho \ln (b/a)}{2 \pi l_2} \qquad (20)$$

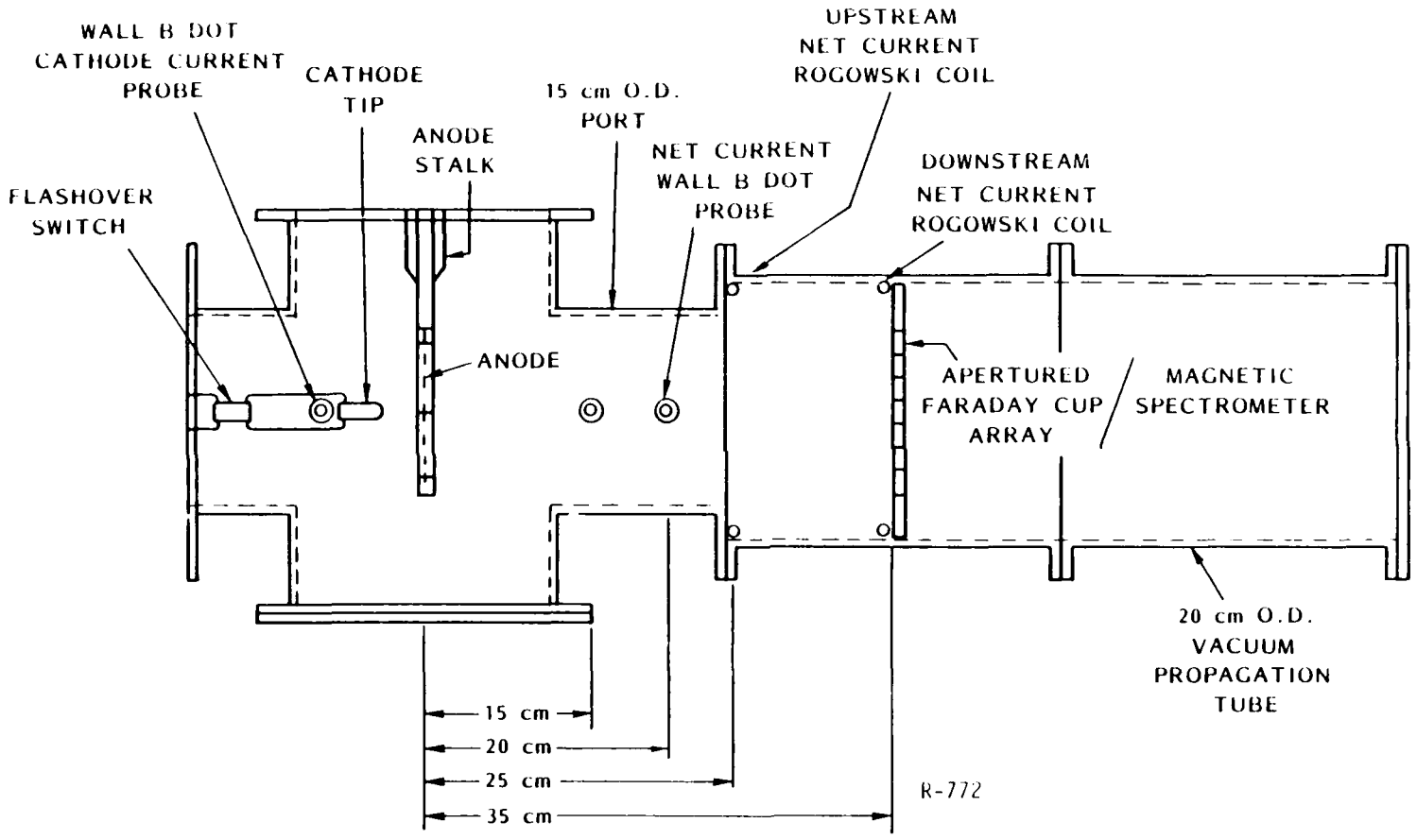

Figure 19. Plasmoid diagnostic configuration.

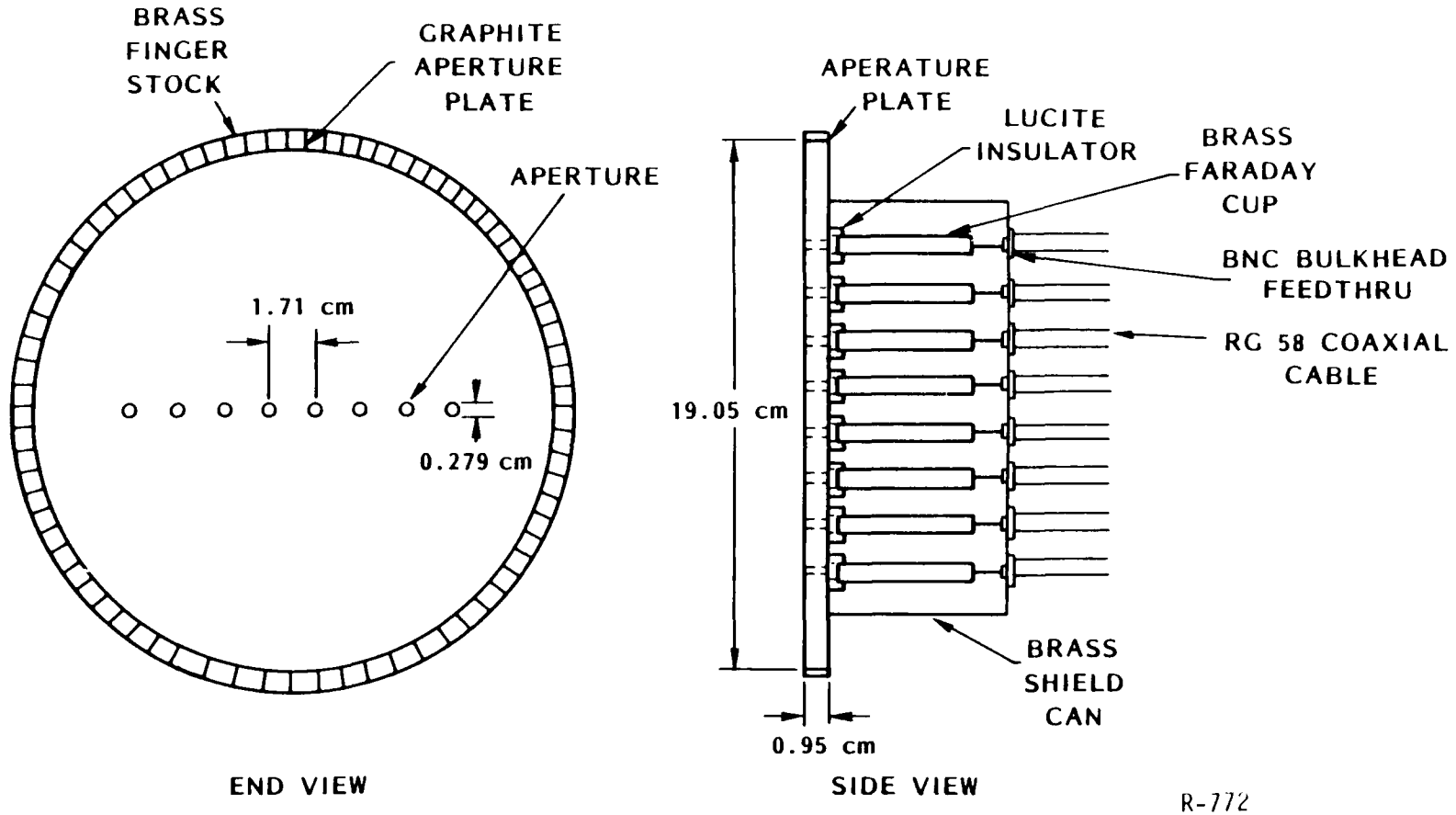

Figure 20. Apertured Faraday cup array.

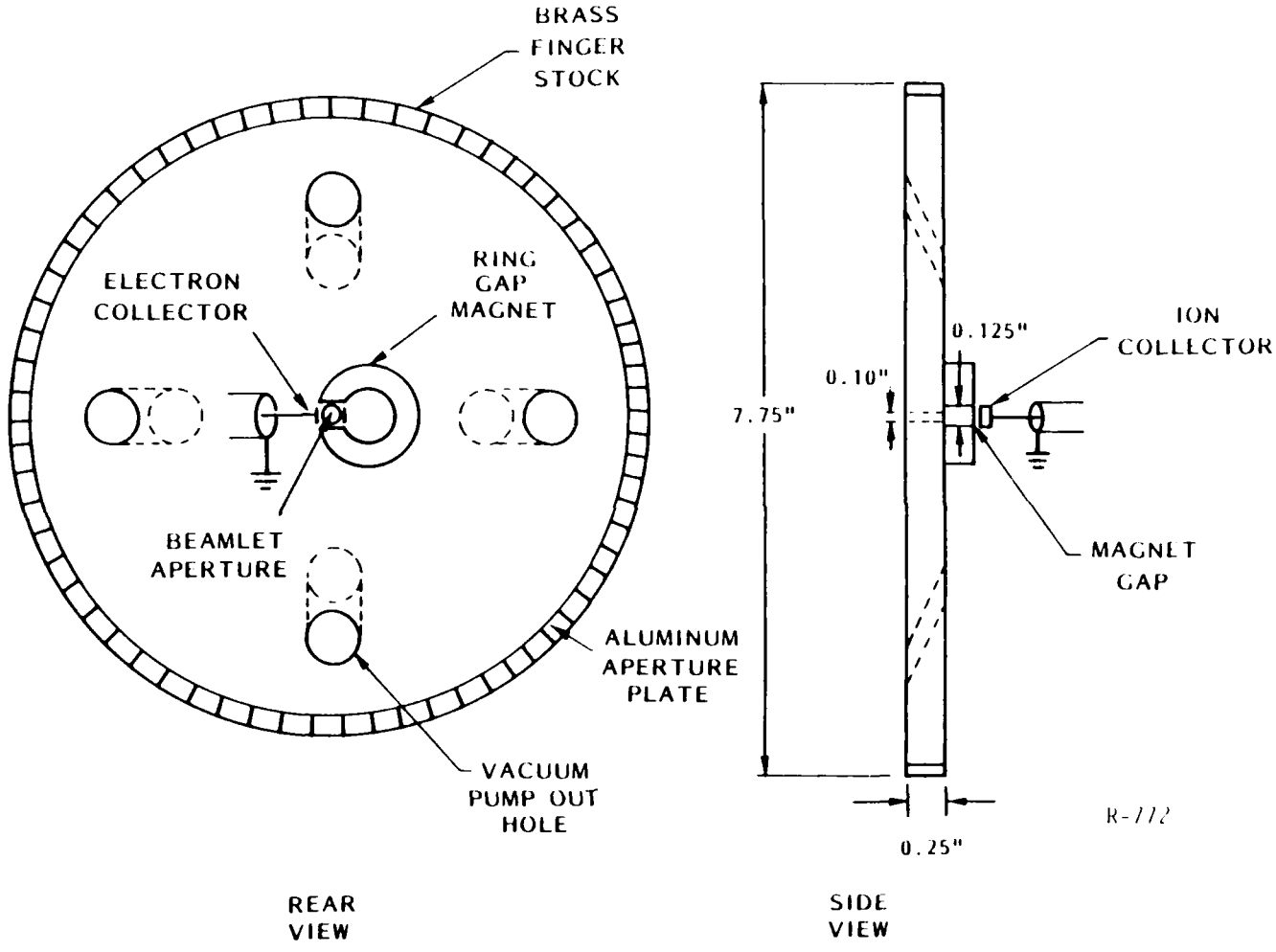

Figure 21. Magnetic spectrometer.

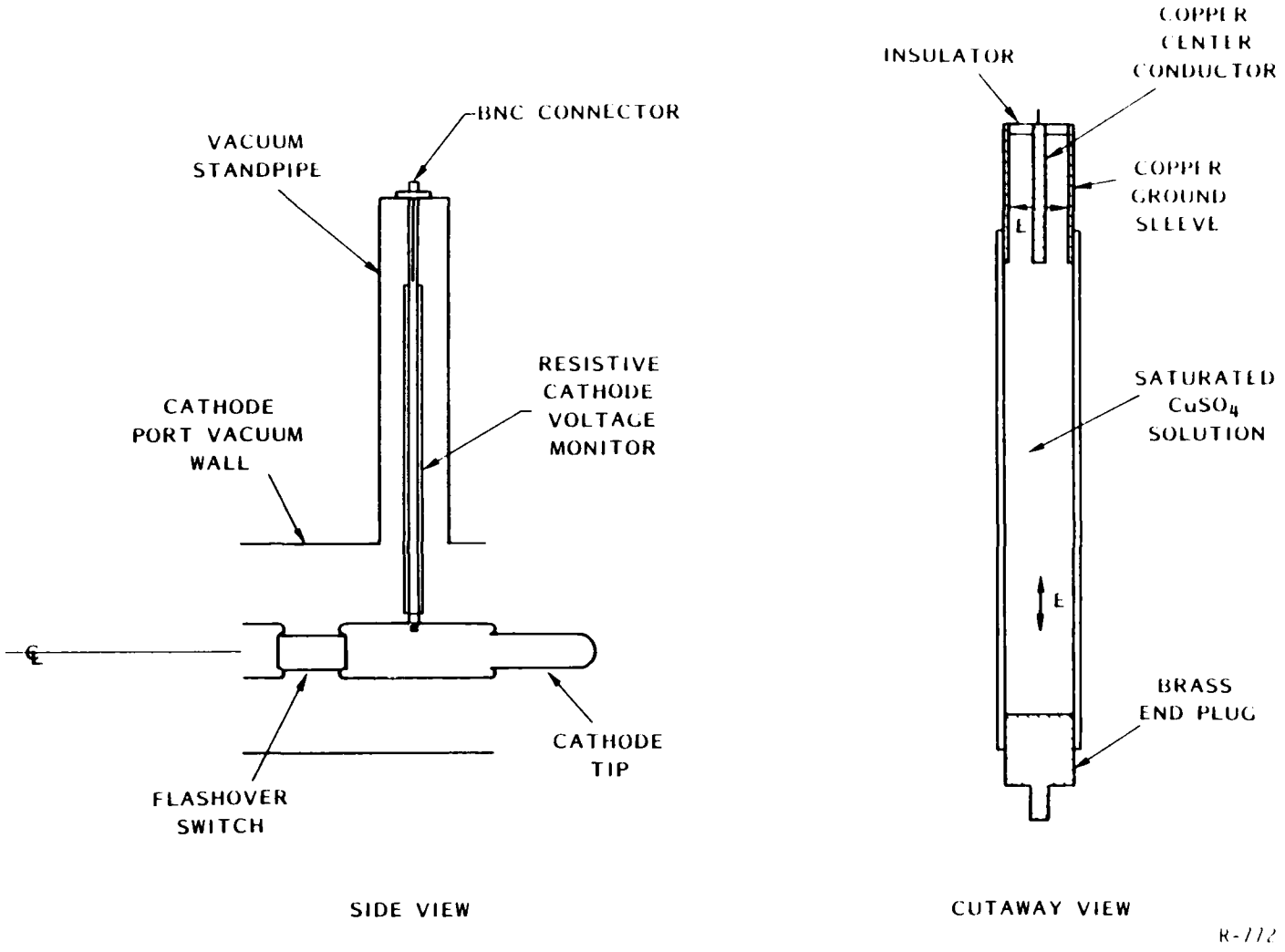

Figure 22. Cathode resistive voltage monitor.

where l_2 is the tube length and a and b are the inner and outer radii, respectively. ρ is the folume resistivity. This geometry can have appreciable capactiance, given by

$$C = \frac{2 \pi \varepsilon l_2}{\ln (b/a)} \tag{21}$$

where ε is the permittivity. For design purposes, we use the relative permittivity of water (80), since the resistive solution is aqueous copper sulfate solution. The "hot" side resistor is just a long insulating tube (Tygon) filled with copper sulfate solution. The DC division ratio for this monitor is simply the division ratio in the absence of the parallel capacitance, and the rise time (for unit step voltage input) is the RC time constant formed by the parallel combination of the two resistors and the coaxial capacitance. By allowing mixing between the two resistor chambers, one can achieve a division ratio which depends on geometry and is independent of resistivity, which is adjusted by the strength of the copper sulfate solution.

We also built a Thomson parabola ion spectrometer (Ref. 14) to examine plasma ion species and verify energies. The Thomson parabola spectrometer uses parallel electrostatic and magnetostatic fields, as shown in Figure 23, to deflect ions in two orthogonal directions. The magnetic deflection angle is given by

$$\tan \theta_m = \frac{Ze\int Bdl}{P} \quad , \tag{22}$$

where P is the particle momentum and $\int Bdl$ is the path integral of the magnetic field through the instrument

The electric deflection is given by

$$\tan \theta_e = \frac{Ze\int Edl}{2T} \quad , \tag{23}$$

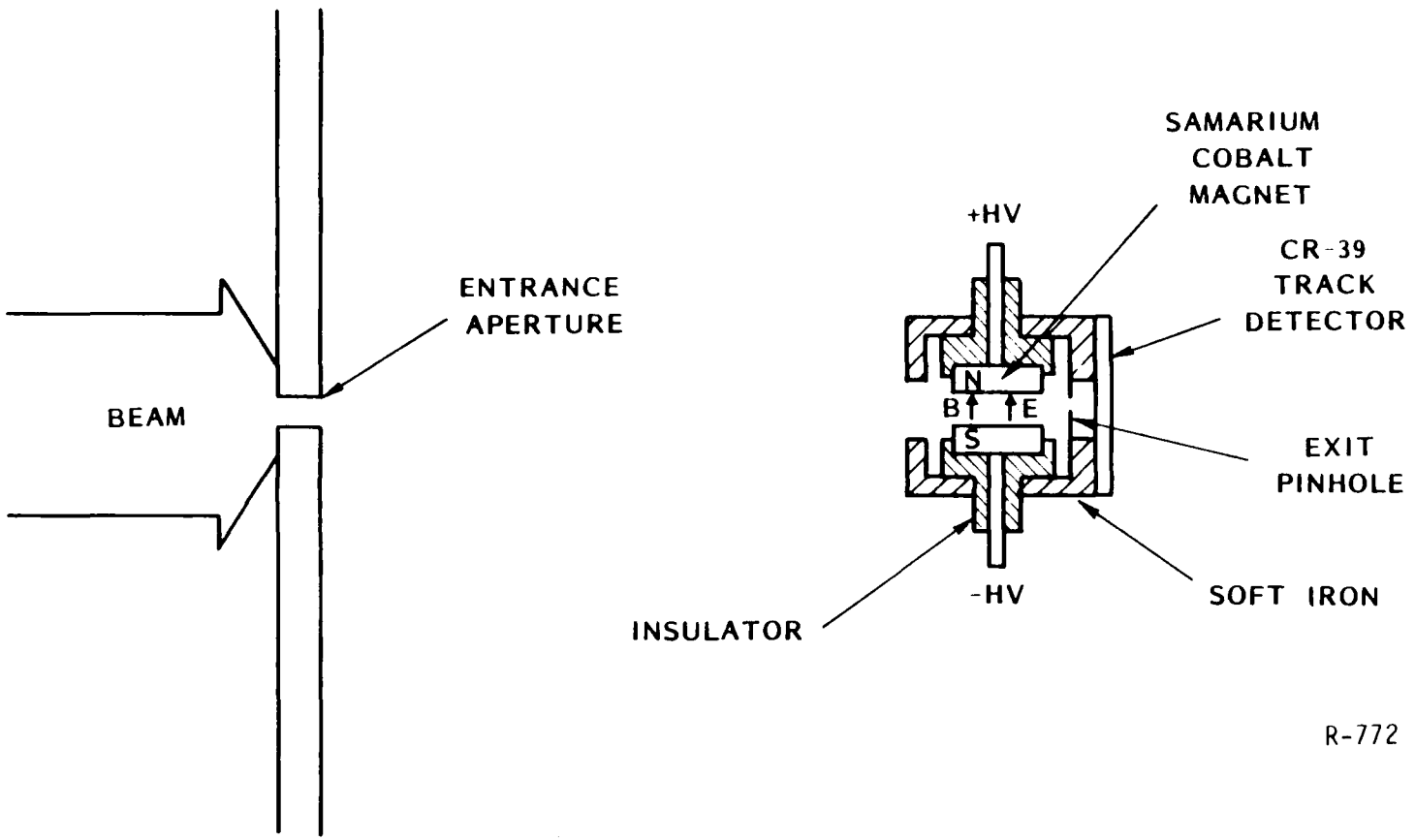

Figure 23. Thomson parabola ion spectrometer.

where T is the kinetic energy of the particle, and $\int Edl$ is the path integral of the transverse electric field through the instrument. The spectrometer thus separates ions of differing charge-to-mass ratios and their projections on a planar target, such as CR-39, are parabolas with a common vertex.

3. DIODE OPERATION

The plasmoid diode operates in the following manner. First, the storage capacitors for the anode pulser (Pulserad 112A) and cathode pulser are charged to high voltage. Next, a command trigger is sent to the 112A Marx generator switch initiating discharge of the capacitors into the coaxial pulse forming line (PFL). Approximately 1 usec after the 112A trigger, another is sent to the cathode pulser spark gap switch, causing its capacitors to discharge through the primary winding of the high voltage transformer, the transformer output charges the cable PFL. Between the PFL output and cathode tip is a 1.75 in long, 1 in diameter dielectric flash-over switch which prevents application of the pulser voltage to the cathode tip until the anode comes up to voltage. This occurs when the 112A's gas-filled over-voltage output switch self-breaks. The high positive potential applied to the anode then capacitively couples to the cathode tip, causing the dielectric switch to short circuit. At this time, strong field emission of electrons occurs at the cathode tip. As the accelerated electrons pass through the anode, a plasma forms from which ions (protons) are extracted and accelerated.

For most shots, a 'foilless' ion diode configuration was employed. That is, rather than having a fixed ground screen electrode downstream of the anode, the near-zero potential within the drift port was used to accelerate the ions (and decelerate the electrons). The cathode was a 1.1 cm diameter planar tip, covered with velvet cloth to improve emission characteristics (Ref. 13). To achieve simultaneity, the exact length of the flashover switch was optimized to the anode voltage, A-K gap distance, and cathode size. When tuned, simultaneity was excellent, with cathode current turn-on occurring within 2 nsec of anode voltage, as shown in Figure 24.

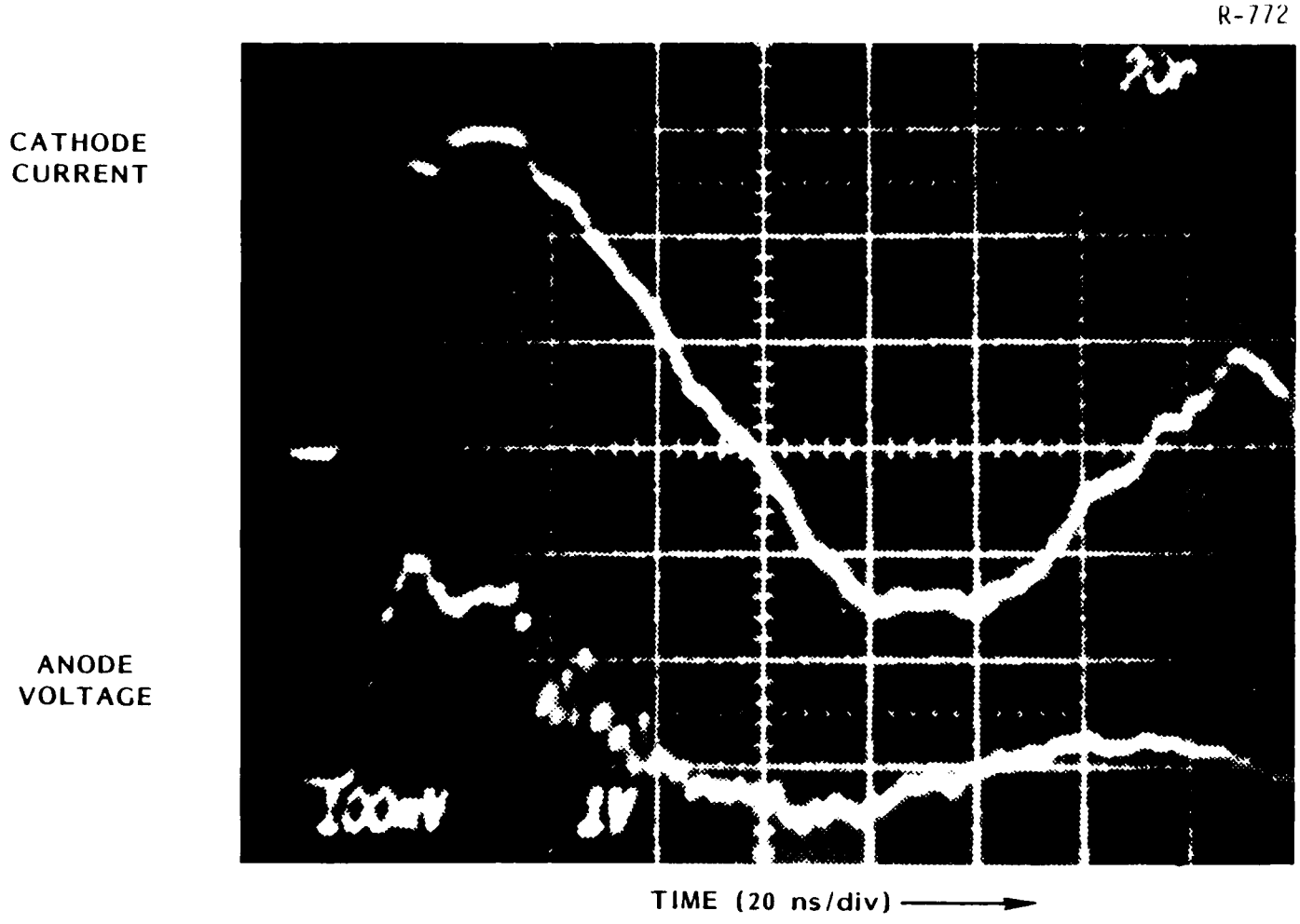

Figure 24. Anode/cathode simultaneity; upper trace: cathode current, lower trace: anode voltage, both at 20 ns/cm.

One occasional problem which adversely affected the operation of the diode was the finite turn-on time of the anode. That is, space charge limited emission of ions from the anode can not begin until formation of plasma. This process was found to take as long as 20 nsec, so that, although voltage simultaneity was achieved, ion current simultaneity was not. Evidence of the ion current delay was seen in the time-resolved impedance of the diode. If electron and ion current flow between the cathode and the anode is space charge limited, the net current is approximately a factor of two higher than the electron space charge limited current in the absence of bipolar flow (Ref. 9). It became clear that at about 12 nsec into the pulse, a shift from unipolar to bipolar flow appeared, indicating, the beginning of ion current.

Unfortunately, we were never able to obtain reliable cathode voltage measurements. Introduction of any voltage probes into the diode region resulted in highly asymmetric current paths at best, and severe arcing at worst.

Lack of a reliable cathode voltage monitor complicated the analysis of the diode performance. Nevertheless, we were able to infer the cathode voltage, assuming a simple resistive divider consisting of the cathode pulser line impedance (4Ω) in series with the diode impedance. Since the voltages at the cathode pulseline and anode were known and the diode current was known, calculation of the cathode potential was straightforward. We found that due to the large anode potential (typically 0.5 MV), the effective cathode potential was only a fraction (typically 0.1 - 0.5) of the applied pulser voltage, or on the order of 10 - 50 kV. Diode currents were approximately 10 - 20 kA, and diode impedances were roughly 20 - 40 Ω, resulting in a near matching of the 112A. The inferred proton and electron terminal velocities, from conservation of energy, are approximately .03c - .04c and .2c - .5c, respectively. Note that at these low electron energies, the theory would indicate that for radial equilibrium downstream, one would expect the ratio of ion to electron current to be just slightly less than the corresponding velocity ratio, and the required area ratio of the two beams to be approximately one.

IV. RESULTS AND DISCUSSION

To diagnose plasmoid propagation, considerable emphasis was placed on downstream net current measurements. It was felt that downstream measurements would be a good indicator of actual electron current associated with the plasmoids since ion current should be a small fraction. Furthermore, since the diode currents were orders of magnitude greater than the space charge limited currents for either electrons or ions in the propagation tube, downstream currents higher than the space charge limits would indicate significant ion densities and, therefore, plasmoid transport.

The majority of the net current measurements were made at a distance 20 cm downstream from the anode within the 15 cm diameter propagation port. A small wall-mounted B_θ-dot loop with subnanosecond rise time was used for these measurements. Wall-mounted Rogowski coils were also fielded at distances further downstream within the 20 cm diameter pipe and supplemented the B_θ-dot loops. It was found that the Rogowski coils were extremely prone to RF noise problems, and their signal-to-noise ratio was too small, rendering them useless.

Typical net current traces from the 20 cm probe are shown in Figure 25 for a 1.9 cm A-K gap shot and Figure 26 for a 0.64 cm A-K gap shot, together with other electrical diagnostics. The peak net currents for these two cases are 2.13 kA and 3.75 kA. Note that for electron energies less than 100 keV and wall-to-beam radius ratios greater than a few, these net currents represent space charge limited current enhancements of at least 20 and 35, respectively. Thus, it may be concluded that significant plasmoid propagation had occurred in both cases. In fact, using the well-characterized parameters for the 1.9 cm A-K gap shot, we found that an ion current of approximately 0.16 kA must have been present. The inferred ion-to-electron current ratio is 0.074. This ratio is in excellent agreement with the predicted current ratio range $0.065 < f < 0.080$, obtained from radial equilibrium arguments.

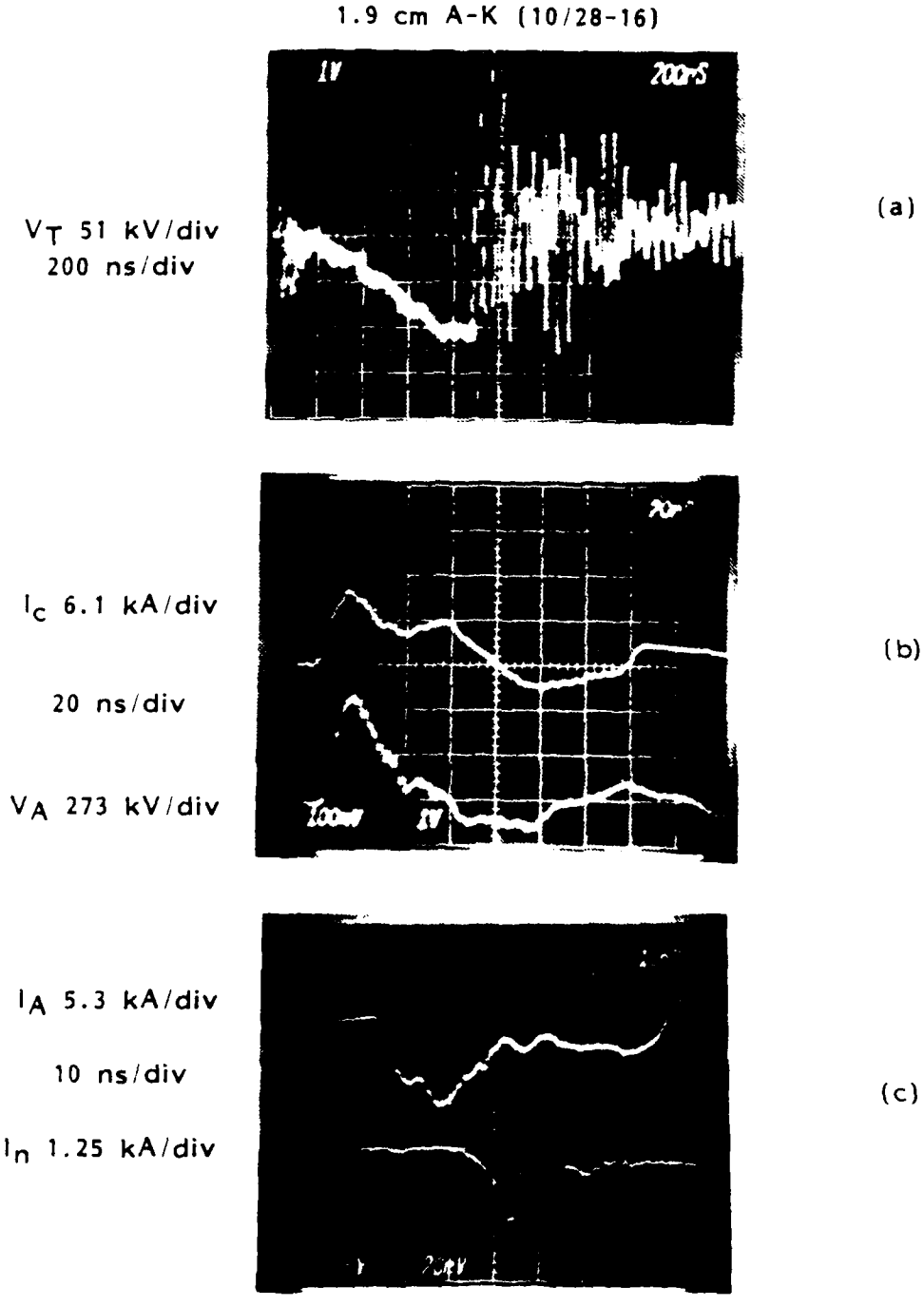

Figure 25. Voltage and current oscillosgrams for a 1.9 cm A-K gap shot. (a) Cathode pulseline voltage, 51 kV/div 200 nsec/div, (b) cathode current (upper), 6.1 kA/div, 20 nsec/div, anode voltage (lower), 273 kV/div, (c) anode current (upper), 5.3 kA/div, 10 nsec/div, downstream net current (lower), 1.25 kA/div.

The net current traces in Figures 25 and 26 also provide us with a check of ion energetics from the delay of net current with respect to diode current. In Figure 26(b), one can see the ion current turn on at approximately 20 nsec into the pulse. At this time, the anode voltage is about 520 kV, corresponding to an ion velocity of 1.0×10^7 m/sec. Thus, the ions should arrive at the 20 cm downstream position about 40 nsec after the beginning of diode voltage and current. In Figure 26(c), the net current is displayed on the same oscilloscope as the anode current, and one can see that the net current delay is, in fact, about 40 nsec.

In Figure 26(b) there is no evidence of delay in the onset of ion current--the voltage and current track each other, implying constant impedance. For this shot, the anode voltage pulse is triangular, with a voltage ramp imparting kinetic energy to the ions at the rate of approximately $\alpha = 1.1 \times 10^{-6}$ J/sec. Since the ion velocity is proportional to the square root of the energy (or voltage), one can write a simple expression for the arrival time of ions at a distance 'd' downstream from the anode. It is:

$$\tau = t_o + d \; / \; \sqrt{2\alpha t_o / m} \tag{24}$$

where t_o is the time at which the ions are created. Since the ions born early in the pulse have slower velocities, they may be overtaken by ions created later with higher velocities. The minimum arrival time can be estimated by differentiating τ with respect to t_o and equating to zero. When this is done, it is found that the time of arrival for the first ions at the downstream location is given by

$$\tau = \frac{3}{2} \left(\frac{md^2}{\alpha}\right)^{1/3} \tag{25}$$

for ions created at time

$$t_o = \frac{1}{2} \left(\frac{md^2}{\alpha}\right)^{1/3} \tag{26}$$

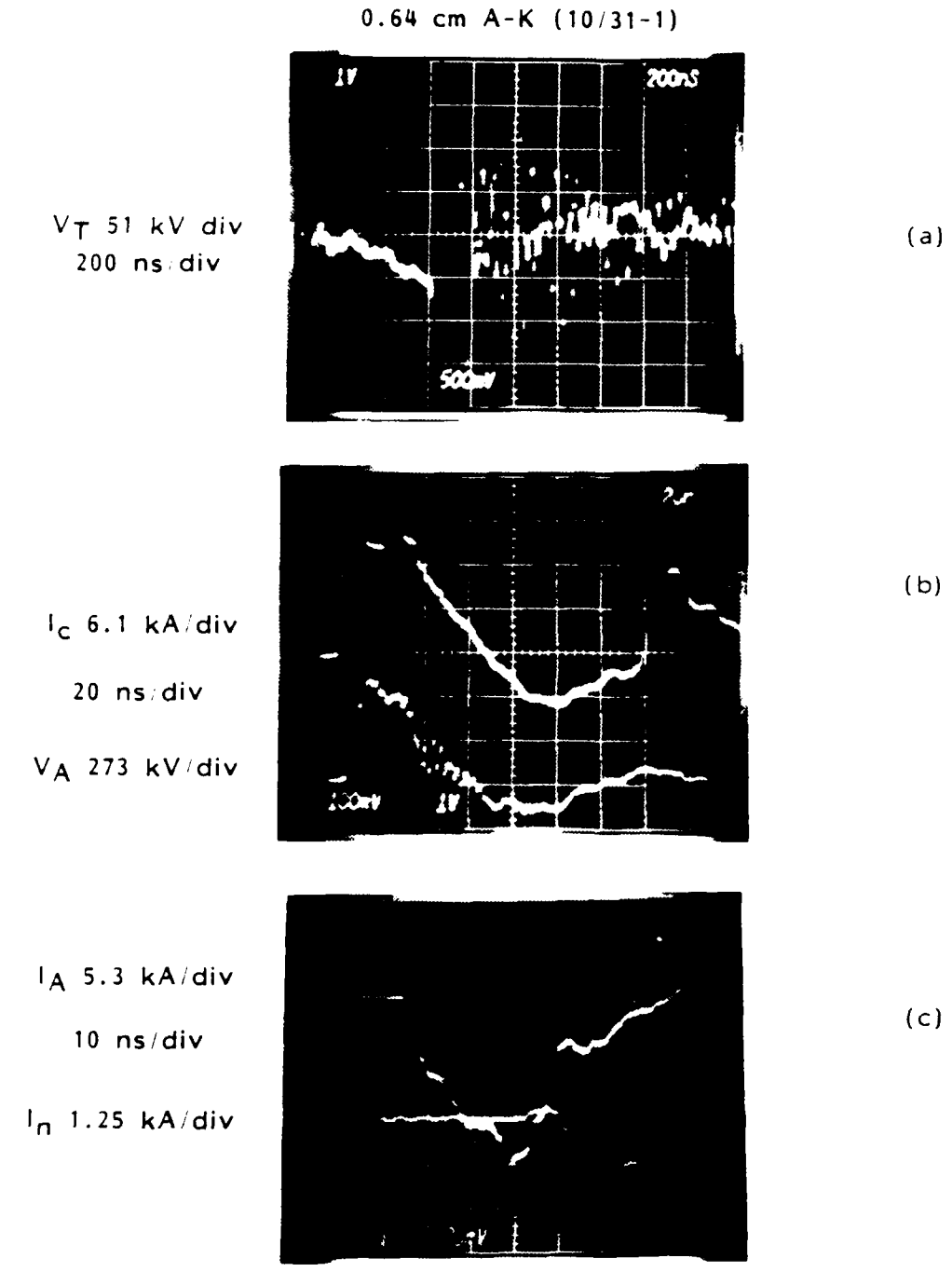

Figure 26. Voltage and current oscillograms for a 0.64 cm A-K gap shot. (a) Cathode pulseline voltage, 51 kV/div 200 nsec/div, (b) cathode current (upper), 6.1 kA/div, 20 nsec/div, anode voltage (lower), 273 kV/div, (c) anode current (upper), 5.3 kA/div, 10 nsec/div, downstream net current (lower), 1.25 kA/div.

When the distance of the net current monitor, d = 20 cm, is substituted with x and the proton mass, one finds that the estimated time of arrival is approximately 27 nsec after the beginning of the diode voltage and current. From Figure 25(c), one can see that the measured delay is about 24 nsec--again, in excellent agreement.

The magnetic spectrometer was employed at a downstream position of 35 cm from the anode. The entrance aperture was 0.05 cm^2 in area. For a charged particle traversing a region of transverse magnetic field, the angle of deflection with respect to its initial path is given by Equation 22. For protons of energy 0.5 MeV, the deflection angle is seen to be negligible, whereas for electrons of energy 0.1 MeV or less, the deflection is sufficient to cause impingement on the side collection electrodes. In general, inferred peak current densities on axis were approximately 10 - 15 A/cm^2 for electrons and 1 A/cm^2 for ions. These values are roughly consistent with estimates based on Bennett profile beams with kA-level currents and a few centimeters radius. The strong positive signals measured by the diagnostic were a further indication of ion transport.

The apertured Faraday cups were also placed in the beam line at the 35 cm downstream position. The unfolded current density radial profiles for a typical shot are shown in Figure 27. The inferred peak net current density was in agreement with the spectrometer data ignoring secondary electron contributions. Note, also, that the profile is centrally peaked with a FWHM radius of a few centimeters. This type of profile was observed for almost all shots. In addition, an offset in the beam center was consistently observe--in the same preferential direction. Upon careful examination of the setup, it was concluded that the displacement was due to the asymmetric anode feed.

The analysis and characterization of the field-free vacuum propagation of the nonneutral plasmoids were hampered by lack of a direct cathode voltage measurement, limited propagation distances due to physical constraints, and occassional RF noise levels. Nevertheless, a basic understanding emerged, supported in a consistent fashion by the various

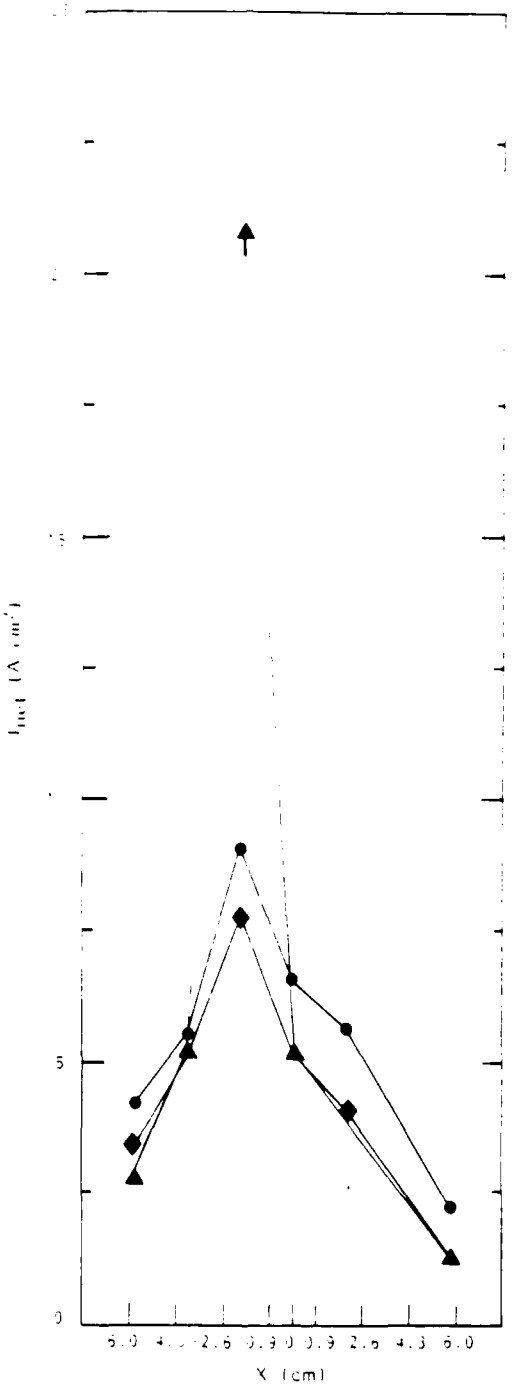

Figure 27. Inferred radial current density profile at two specific times and time-averaged at Z = 35 cm downstream.

theoretical consi erations and diagnostic measurements. To summarize, the plasmoid diode behaved as anticipated, although in some cases ion current was delayed with respect to electron current. We believe this delay was due to finite anode plasma formation time, and is certainly a function of electron current density and voltage as well as physical details of the anode. The electron and ion beams generated in the diode were well above the space charge limited currents for either specie within the propagation tube and do not, in general, support a radial equilibrium. It appears that the beams 'adjust' by shedding excess particles depending on the instantaneous local fields until equilibrium is achieved. The entire assembly then propagates in a coherent manner at the ion axial velocity, with the faster electrons continuously emerging through the beam head and leaving the system due to space charge repulsion. The beams thus propagating can be more than an order of magnitude greater in current than either electrons or ions individually.

V. CONCLUSIONS AND RECOMMENDATIONS

The work described in this report has led to an enhanced understanding of nonneutral plasmoid generation and propagation. Since it is the first experimental investigation of its kind, it has also resulted in identification of potential new technology as well as problem areas requiring further study. The conclusions that can be drawn from the study are summarized as follows.

1. The simple analytical radial equilibrium considerations for charge- and current-nonneutral plasmoids appear to be substantiated qualitatively by experiment; equilibrium does not require charge and current neutrality.

2. The Virtual Cathode Ion Diode is potentially a very effective device for the production on nonneutral plasmoids, based on one-dimensional analysis.

3. The use of spiral air-core transformers and solid dielectric pulse lines can result in extremely compact (high energy density) pulsed power systems.

4. Compound diodes with transmission anodes based on the VCID principle can be operated with independent pulsed power supplies, provided that adequate vacuum insulation is available.

5. The generation of large quantities of free ions for acceleration is delayed due to non-zero plasma formation time; this delay is approximately 10 nsec for the parameters of our experiments.

The single greatest impediment to the successful achievement of the goals of this study was the lack of suitable pulsed power drivers. Specifically, for long-distance and cross-field propagation studies much longer pulse lengths are required. Thus, if this work is continued, new drivers will have to be located or developed. In addition, symmetrically-fed, large-volume diodes will have to be designed and constructed.

One of the most promising aspects of this work was the identification and preliminary analysis of the Virtual Cathode Ion Diode. The device has relevance to such areas as ion/plasma propulsion systems as well as the

generation of actively neutralized ion beams for directed energy applications. A small-scale experimental/simulation effort is recommended which evaluates in detail the capabilites of the VCID.

Finally, some thought concerning the inherent mass disparity in conventional plasmoid species has led us to consider schemes resulting in equal, or nearly equal, mass specie plasmoids. One possible approach is to create plasmoids from salts such as NaF, KCl, or CsI. Due to the complementary electron structure of these ion pairs, it is conceivable that singly charged positive and negative ions could be produced with mass differences ranging from 19 percent (NaF) down to 5 percent (CsI). A second, more exotic approach is to create electron/positron pairs for acceleration. At least conceptually, this could be achieved with a very-high-energy electron beam interacting with a high-Z material to produce high-energy bremsstrahlung with resultant pair production.

REFERENCES

1. Bostick, W. H., Phys. Rev. Lett. 104, 292, 1956 (Unclassified).

2. Humphries, S., Jr., Lockner, T. R., Poukey, J. W., and Quintenz, J. P., Phys. Rev. Lett. 46, 995, 1981 (Unclassified).

3. Adler, R. J., Nation, J., and Sevlin, V., Phys. Fluids 24, 347, 1981 (Unclassified).

4. Adler, R. J., J. Appl. Phys. 52, 3099,1981 (Unclassified).

5. Floyd, L. E., Destler, W. W., Reiser M., and Shin, H. M., J. Appl. Phys. 52, 693, 1981 (Unclassified).

6. Destler, W. W., O'Shea, P. G., and Reiser, M., Phys. Fluids 27, 1897, 1984 (Unclassified).

7. Bennett, W. H., Phys. Rev. Lett. 45, 890 1934; Phys. Rev. Lett. 98, 1584, 1955 (Unclassified).

8. Kiuttu, G. F., Adler, R. J., and Humphries, S., Jr., "MRC Virtual Cathode Ion Diode Development: Part I - 20-Specie Non-Relativistic 1-D Planar Space Charge Limited Flow (U)," AMRC-N-288, Mission Research Corporation, February 1985 (Unclassified).

9. Poukey, J. W., Appl. Phys. Lett. 26, 145, 1975 (Unclassified).

10. Bogdankevich, L. S., and Rukhadze, A. A., Sov. Phys. Uspekhi 14, 163, 1971 (Unclassified).

11. Thompson, J. R., and Sloan, M. L., Proceedings of the 2nd International Conference on High Power Electron and Ion Beam Research and Technology, Vol. II, (Laboratory for Plasma Studies, Cornell University, Ithaca, New York, 1977), pp. 729-740; Sullivan, D. J., and Coutsias, E. A., "Theory and Application of the Virtual Cathode in Charged Particle Beams (U)," AMRC-R-433, Mission Research Corporation, December 1982 (Unclassified).

12. Cook, E., and Reginato, L., Proc. of the 13th Pulsed Power Modulator Symposium (U), Buffalo, New York, pp.27-33, June 1978 (Unclassified).

13. Adler, R. J., Kiuttu, G. F., Simpkins, B. E., Sullivan, D. J., and Voss, D. E., Rev. Sci. Instrum. 56, 76, 1985 (Unclassified).

14. Rhee, M.J., Rev. Sci. Instrum. 55, 1229, August 1984 (Unclassified).

VI. APPENDIX

A. PUBLICATIONS, REPORTS, AND PRESENTATIONS

The following papers related to this work have been submitted for publication:

"The Virtual Cathode Ion Diode," G. F. Kiuttu, R. J. Adler, and S. Humphries, Jr., recommended for publication in Applied Physics Letters, pending revision.

"Production and Propagation of Nonneutral Plasmoids," G. F. Kiuttu, R. J. Adler, and M. K. Williams, accepted for publication in the Proceedings of the Sixth International Conference on High-Power Particle Beams, Kobe, Japan, edited by C. Yamanaka, Institute of Laser Engineering, Osaka University, pp. 291-294, 09-12 June 1986 (U).

"Nonneutral Plasmoid Generation and Propagation," G. F. Kiuttu and R. J. Adler, accepted for publication in Proceedings of the SPIE Symposium on Innovative Science and Technology, Los Angeles, California, 10-15 January 1988 (U).

The following internal reports have been prepared under this contract:

"MRC Triode Development: Part I, Non-Relativistic 1-D Planar 2-Specie Space Charge Limited Flow," AMRC-N-288, G. F. Kiuttu, R. J. Adler, and S. Humphries, Jr., February 1985 (U).

"Research Progress and Forecast Report: Plasmoid Propagation," AMRC-R-712, G. F. Kiuttu and R. J. Adler, May 1985 (U).

"Interim Annual Report: Plasmoid Propagation," AMRC-R-722, G. F. Kiuttu and R. J. Adler, May 1986 (U).

In addition, the following papers have been presented at the indicated meetings or conferences:

"B_θ Confined Plasmoid Experiment," G. F. Kiuttu and R. J. Adler, presented by G. F. Kiuttu and R. J. Adler at the First Meeting of the New Mexico Association for Plasma Propagation, Sandia National Laboratories, December 17, 1984.

"Virtual Cathode Ion Diode," G. F. Kiuttu, R. J. Adler, and S. Humphries, Jr., 1985 IEEE International Conference on Plasma Science, Pittsburgh, June 3-5, 1985.

"Plasmoid Production and Propagation - Theoretical Aspects," G. F. Kiuttu, R. J. Adler, and S. Humphries, Twenty-Seventh Annual Meeting of the Division of Plasma Physics of the American Physical Society, San Diego, November 4-8, 1985.

"Plasmoid Production and Propagation - Experimental Aspects," M. K. Williams, R. J. Adler, G. N. Estepp, and G. F. Kiuttu, Twenty-Seventh Annual Meeting of the Division of Plasma Physics of the American Physical Society, San Diego, November 4-8, 1985.

"Production and Propagation of Nonneutral Plasmoids," G. F. Kiuttu, R. J. Adler, and M. K. Williams, Sixth International Conference on High-Power Particle Beams, Kobe, Japan, edited by C. Yamanaka, Institute of Laser Engineering, Osaka University, pp. 291-294, 09-12 June 1986 (U).

"Nonneutral Plasmoid Generation and Propagation," G. F. Kiuttu and R. J. Adler, SPIE Symposium on Innovative Science and Technology, Los Angeles, California 10-15, January 1988 (U).

APPENDIX B

PRODUCTION AND PROPAGATION OF NONNEUTRAL PLASMOIDS

PRODUCTION AND PROPAGATION OF NONNEUTRAL PLASMOIDS

G. F. Kiuttu, R. J. Adler† and M. K. Williams

Mission Research Corporation
1720 Randolph Road, S.E.
Albuquerque, New Mexico, USA

Abstract

Simple analysis has predicted that for certain regimes in current, radius, and velocity parameter space, radial equilibrium of costreaming electron and ion beams can be expected. Neither charge nor current neutrality is required. We have begun experiments to study such nonneutral plasmoids. The key to producing them is independent pulsed power sources for each beam. Typical operating parameters for our experiments are electron and ion (proton) energies of 100 KeV and 1 MeV, respectively, and currents of 2 kA and 200 A, respectively. The observed currents are roughly an order of magnitude greater than the single specie space charge limiting currents within the 10 cm radius drift tube. Current density profiles are centrally peaked with characteristic radii of a few centimeters. Diagnostic measurements suggest that the faster electron beam moves continuously through the ions and blows up radially as it emerges ahead of the ion front. In this paper we present a description of the experiment and results to date.

Introduction

For a wide variety of applications ranging from industrial ion implantation to inertial confinement fusion and space propulsion, it is desirable to have tunable beams of high current density ions. A fundamental issue in the transport of intense charged particle beams is neutralization - both charge and current - since space charge effects can severely limit the maximum particle flux deliverable from one point to another. In particular, for ion beams, electron neutralization is conventionally achieved passively. That is, the beam passes through a region of gas, plasma, or other source of electrons, and the instantaneous local fields draw the lighter electrons into the beam region. In this paper we describe an experiment in which not only active neutralization is employed, but, to a certain degree, the electrons are used to control the ion beam parameters. The motivation for the experiments was a simple analysis which showed that for costreaming uniform coaxial ion and electron beams, pinched beam equilibria for both beams should be expected for certain relative current and charge density ratios [1].

Diode Description

A simplified drawing of the special plasmoid diode used to simultaneously accelerate ions and electrons in the same direction is shown in Fig. 1. As long as the anode can supply ions and remain at least partially transmissive to the electrons, the source potentials dictate net kinetic energy for both species in the grounded drift region. In this diode, the electron beam accelerated across the A-K gap generates an anode plasma which becomes the ion source. In addition, the space charge limited ion current in the diode region depends significantly on the injected electron parameters. A steady-state one-dimensional analysis was carried out for the two specie diode which showed that very modest power electron beam sources could be used to control much higher power ion beams and boost the achievable ion current significantly above the single specie space charge limit [2].

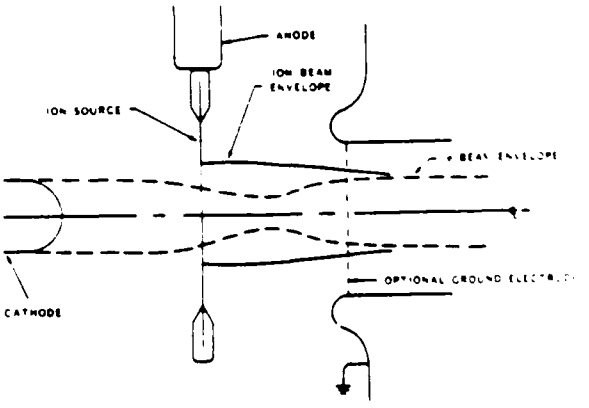

Fig. 1. Plasmoid diode schematic.

The key to realizing such diode operation experimentally is the integration of separate source power supplies for electrons and ions. In our experiments the anode was pulse biased to 0.5-1.0 MV with a Pulserad 112A accelerator configured with a simple coaxial line (20 Ω) for a 30 nsec positive polarity pulse into a matched load. To bias the cathode, a novel compact pulsed power supply was designed and built employing a spiral air core transformer [3] in conjunction with a solid dielectric cable pulseline [4]. A schematic diagram of the pulser is shown in Fig. 2. Maximum output (open circuit) voltage is approximately 500 kV, with a 50 nsec pulse delivered to a matched 4 Ω load.

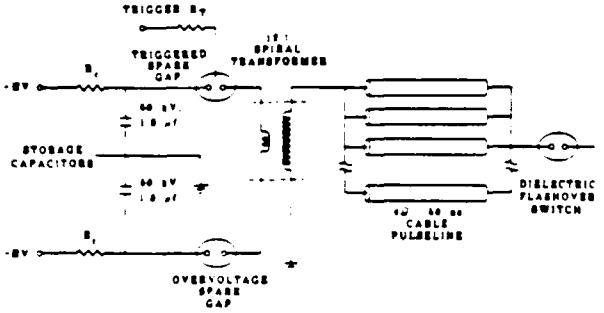

Fig. 2. Plasmoid cathode pulser schematic.

Experimental Results

A drawing of the experiment configuration is shown in Fig. 3. In addition to the diagnostics indicated, resistive voltage dividers were used to monitor the anode and cathode voltages and the anode current was measured with a self-integrating B-dot probe. For the bulk of our experiments, the anode voltage was in the range 0.4-0.7 MV, and the cathode voltage was varied between 0 and 100 kV. A complete set of diode electrical diagnostic signals is shown in Fig. 4 for a 1 cm A-K gap, 1 cm^2 cathode shot. With the solid dielectric flashover switch in the cathode shank (shown in Fig. 3), excellent simultaneity of anode and cathode voltages was achieved. As indicated by the oscilloscope traces, for this diode configuration, total currents were on the order of 10 kA. The net current measured by a wall-mounted fast B-dot probe at 20 cm downstream was slightly more than -1 kA. The space charge limited current for an electron beam within the drift tube is approximately 100 A, an order of magnitude lower. The high net current implies a neutralizing proton current of approximately 100 A - also considerably higher than the ion space charge limit for this geometry. In our experiments, net currents as high as 5 kA were observed which indicate electron and ion currents more than an order of magnitude above their respective single specie space charge limits.

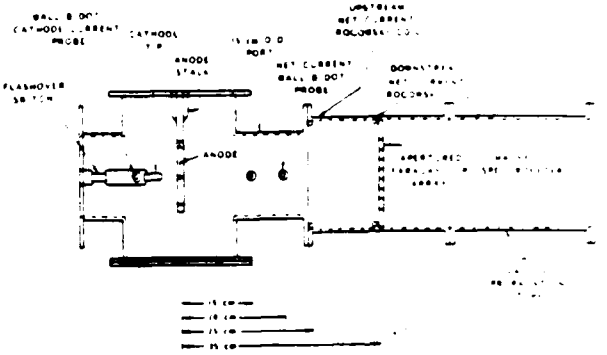

Fig. 3. Diode and diagnostic configuration.

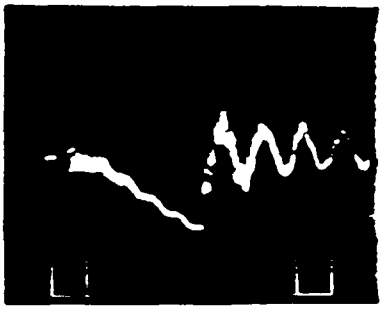

(a)

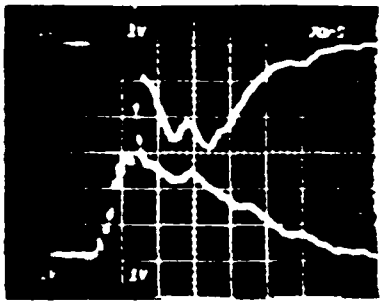

(b)

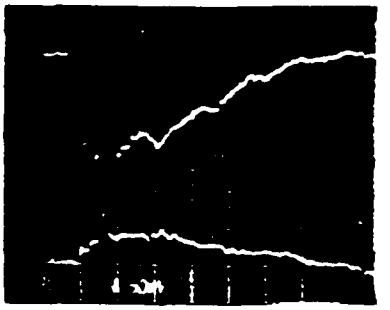

(c)

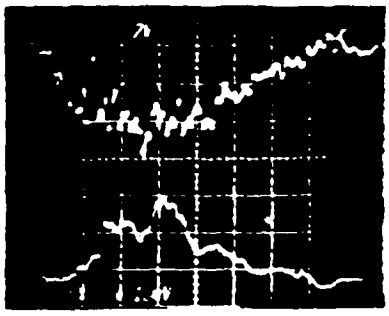

(d)

Fig. 4. Diode electrical signals for a 1 cm A-K, 1 cm^2 cahtode shot.
(a) Cathode pulseline voltage; 33 kV/div, 200 nsec/div.
(b) Cathode tip voltage (top), 17.5 kV/div; anode voltage (bottom), 273 kV/div, 20 nsec/div.
(c) Anode voltage (top), -273 kV/div; cathode current (bottom), -8.7 kA/div, 20 nsec/div.
(d) Anode current (top), -5.3 kA/div; downstream (20 cm) net current (bottom), -0.6 kA/div, 20 nsec/div.

From the relative time of arrival of the plasmoid beam front at the downstream net current probe position, we infer a drift velocity which is essentially the ion drift velocity obtained from conservation of energy (approximately 1 cm/nsec for typical anode voltages). Note that the electron drift velocity is usually a factor of ten greater than this. However, as the faster electrons emerge from the front of the ion beam, the space charge limit is significantly exceeded and the electrons rapidly diverge radially to the wall.

To examine the beam transport further, a linear array of apertured Faraday cups was inserted into the propagation tube at a distance downstream of 35 cm. The time-resolved net current density radial profile was obtained. A plot of the inferred profile at three different times for one shot is shown in Fig. 5. In most cases we observed a centrally peaked profile with a characteristic radius of a few centimeters. We also consistently observed a net transverse displacement of the beam centroid which correlates well with the asymmetric anode feed in the diode. The Faraday cup measurements indicate that a pinched beam equilibrium does in fact exist for these nonneutral beams.

Summary

In summary, we have demonstrated experimentally a new technique for generating nonneutral plasmoids using an active technique for supplying comoving electrons to an ion beam. The ion beam generated depends significantly on the electron parameters. The combined beams have been propagated in vacuum distances of several wall radii, with transport more than an order of magnitude above the single specie space charge limits. The beam front velocity is essentially the ion velocity. The beam current density radial profile is centrally peaked with a radius of a few centimeters.

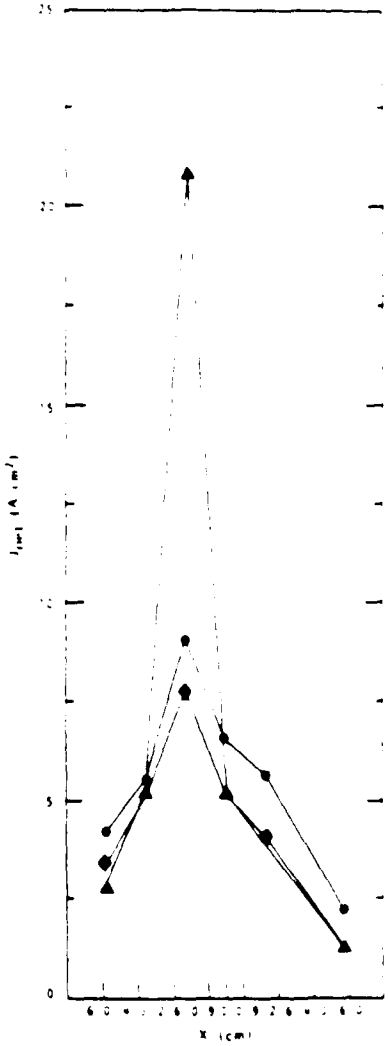

Fig. 5. Inferred current density radial profile at z = 35 cm downstream.

Acknowledgements

The authors wish to express their gratitude to the Air Force Office of Scientific Research of funding this work.

† Pulse Sciences, Inc.
2001 Wilshire Blvd., Suite 600
Santa Monica, CA 90403 USA

References

1. G. F. Kiuttu, R. J. Adler, and S. Humphries, Jr., J. Bull. Am. Phys. Soc. 30, 1391, (1985).

2. G. F. Kiuttu, R. J. Adler, and S. Humphries, Jr., to be published.

3. G. Rohwein, "High Voltage Air Core Pulse Tranformers," Sandia National Laboratory, SAND 80-0451 (1980) (Unpublished).

4. M. K. Williams, R. J. Adler, G. N. Estepp, and G. F. Kiuttu, Bull. Am. Phys. Soc. 30, 1391 (1985).

APPENDIX C

NONNEUTRAL PLASMOID GENERATION AND PROPAGATION

873 32

Noneutral Plasmoid generation and propagation

G.F. Kiuttu and R.J. Adler[1],
Mission Research Corp., 1720 Randolph Rd. SE,
Albuquerque,NM, 87108

ABSTRACT

We have performed an experimental and theoretical study of a simple, axially directed Plasmoid which is neither charge or current neutral. This Plasmoid was produced in a novel virtual cathode ion diode, and subsequently propagated in vacuum. In this paper, we describe the simple theory underlying this type of Plasmoid, and the major results of the experiment.

1. INTRODUCTION

Plasmoids[2] are ensembles of electrons and ions possessing significant directed energy in vacuum. With the development of intense ion beam technology, one can realistically discuss the production of Plasmoids of high kinetic energy (i.e. Megajoules) which have high velocity (~.5c). Plasmoids of this type could potentially be used in ballistic missile defense applications, since large energies are involved and virtually all the Plasmoid energy is absorbed by the target.

In this work, we have performed analytical studies of radial Plasmoid confinement and the behavior of a Plasmoid diode. The Plasmoid configuration[3] we consider is that of two forward directed, beams, one made up of electrons, and one made up of ions, with the electron beam moving faster and having higher density. We have also developed the pulsed power hardware necessary to generate the individual electron and proton beams constituting the Plasmoids under investigation. Finally, we have carried out a series of experiments to actually produce Plasmoids and propagate them over significant distances in vacuum.

We have successfully transported currents more than an order of magnitude higher than the unneutralized (single specie) space charge limited currents for our geometries and energies. Furthermore, the Plasmoids have remained coherent over distances of several drift tube radii as measured by Faraday cup arrays. Maximum net currents measured downstream of the diode have been as high as 5 kA negative, with corresponding ion currents a factor 10-15 lower.

2. THEORY

Two fundamental questions which arise concerning this concept are: 'Can an equilibrium exist for such assemblies?', and 'Can such assemblies be produced?' The first question is addressed in the following section, where it is shown that, on the basis of a relatively simple analysis, equilibrium can be expected for certain parameter regimes of electron and ion velocities and current ratios.

Beams of charged particles propagating in equilibrium usually assume a density profile determined by pressure balance. To simplify analysis and concentrate on the physics of the configuration, we approximate the beam profiles as uniform with uniform axial velocity fields, no transverse energy (cold beam limit), and a beam radius r_b. In this one-dimensional analysis, we examine the net radial forces acting on the outermost particles since the forces are all linear with radius. The other quantities are interest are total currents, I_e and I_i, and axial velocities, v_e and

the dimensionless quantities, $f = -I_j/I_e > 0$, and $\nu = v_j/v_e$, then radial confinement of the plasmoid requires that

$$nf \geq \frac{\nu(1-\beta_e^2)}{(1-\nu\beta_e^2)} \quad , \quad \text{for} \quad n \leq 1, \quad \text{and}$$

$$f \geq \frac{\nu(1-\beta_e^2)}{(1-\nu\beta_e^2)} \quad , \quad \text{for} \quad n \geq 1 \quad .$$

We obtain a geometric mean value for f of

$$\langle f \rangle = \frac{\beta_j \gamma_j}{\beta_e \gamma_e}$$

The expectations for equilibrium are graphed schematically in Figures 1 and 2 for electron velocities of .5c, and .8c respectively.

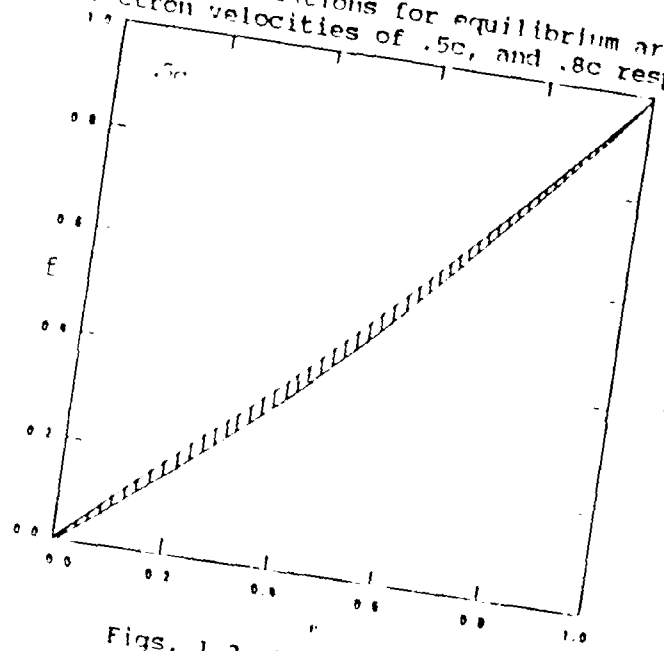

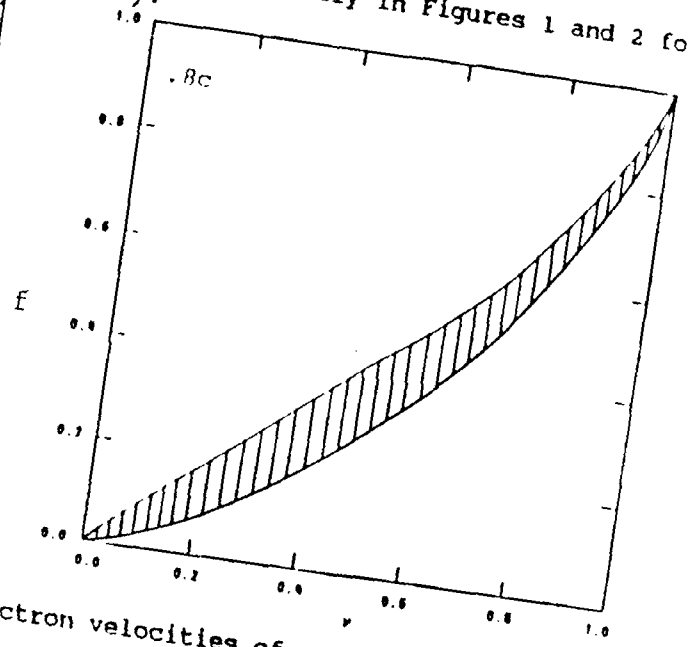

Figs. 1,2. Equilibrium space for electron velocities of .5 and .8c.

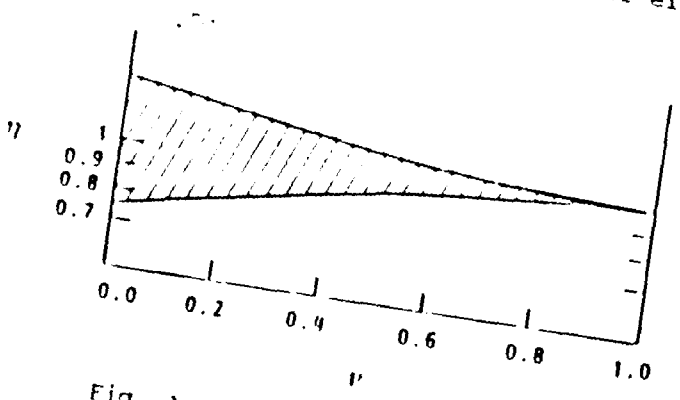

Fig. 3. Relative range of equilibrium.

One can see that the relative size of the area in parameter space corresponding to equilibrium increase as the electron energy increases. We can define an equilibrium figure of merit, $(f_{max} - f_{min})/\nu$, as a quantitative measure of this area. It is graphed for three cases in Fig. 3.

We should point out again that this analysis is quite simple. In reality, the areas corresponding to equilibrium will be diminished, since the radial pressure force due to the non-zero transverse particle energy was neglected in the derivations. A more exact equilibrium analysis would have to take into account temperature effects. Nevertheless, we may conclude that the equilibrium can be achieved, and that the range of equilibrium is wider at higher energy, and therefore easier to achieve.

3. VIRTUAL CATHODE ION DIODE

The Virtual Cathode Ion Diode was conceived as the means of producing non-neutral Plasmoids, and it is shown conceptually in Figure 4. The principle of operation is as follows: An electron beam is injected into a conventional ion acceleration gap with sufficient energy to completely traverse it and emerge at the other side. The presence of the co-moving electron within the gap provides space charge neutralization of the ions to increase the achievable current density. If enough electrons are injected, the potential actually swings negative in the diode. This potential reversal has the beneficial effect of inhibiting electron emission and backflow from the grounded electrode, resulting in very high ion power efficiencies. Since the electrons emerge travelling in the same direction as the accelerated ions, they provide the source of the electron beam.

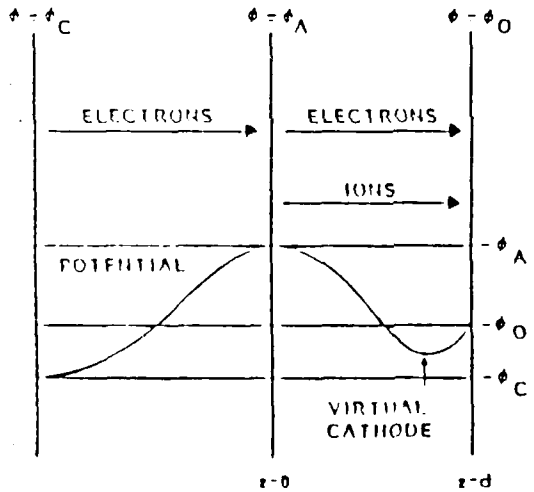

Fig. 4. The potentials in the Virtual Cathode Ion Diode.

We have analyzed the VCID using a one-dimensional, two-specie, steady-state, non-relativistic planar formalism. The boundary conditions for the problem are the fixed electrode potentials and space charge limited particle flow (E = 0) at the anode.

We found that solutions only exist for j_i, j_e, and ϕ_C lying on a particular surface in the three-dimensional parameter space. If we define the normalized (to the single specie Child-Langmuir space charge limiting) current densities then a slice of the parameter solution in the p = 1.1 plane looks like the curve in Figure 5, and $p=(\phi_A-\phi_C)/(\phi_A-\phi_0)$. Point C is just the generalized bipolar flow[4] case ($d\phi/dz = 0$ at the downstream electrode). For this special case, the relationship between the normalized current densities is

$$j_i = j_e \left[p^{1/2} - (p-1)^{1/2}\right]$$

As one proceeds along the curve from point C, the potential barrier rises monotonically, until E, where the potential barrier equals the incident electron energy. It is in the region between point C and E where the VCID operates.

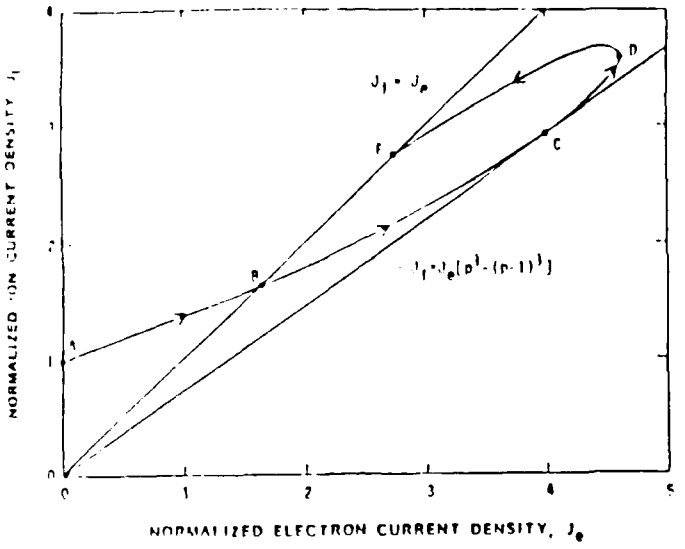

Fig. 5. Solution curves for p=1.1.

If we define the ion power efficiency for the diode as

$$\eta_p = \frac{J_i(\phi_A-\phi_0)}{J_i(\phi_A-\phi_0) + J_e(\phi_0-\phi_C)}$$

then one can see, from Figure 5, that for the same lower bound operating point, extremely high efficiencies are possible.

IV. APPARATUS AND DIAGNOSTICS

The pulse power source for the ion beam was the Pulserad-112A accelerator. The output parameters for the accelerator were 1.6 MV maximum open circuit voltage, 20 line impedance, and a 30 nsec pulse length into a matched load.

To pulse bias the cathode independently of the anode for the experiments, a second, transformer-based line-type pulser was built. The impedance of the cable is nominally 50 Ohms. To reduce the line impedance, twelve 17 ft long cables were connected in parallel, giving an effective line impedance of about 4 Ω and a pulse length of 50 nsec into a matched 4Ωload.

The most important part of the experimental setup is the diode illustrated schematically in Figure 6. Within this region, voltages of hundreds of kilovolts and durations of only tens of nanoseconds from the two pulsers had to be applied simultaneously for proper operation. This was achieved by inserting a dielectric surface flashover switch in the cathode stalk just before the tip. The geometry was chosen so that when the cathode pulser fired, the switch would hold off the maximum pulser voltage, but break down rapidly when the capacitively coupled anode voltage was applied.

Several diagnostics were used in the course of the experiments to determine the characteristics of Plasmoid formation and propagation. These included resistive voltage monitors, B-dot and Rogowski coil current monitors, an apertured Faraday cup array or net current density current profile measurement, and a magnetic particle spectrometer for determining separate ion and electron densities on axis.

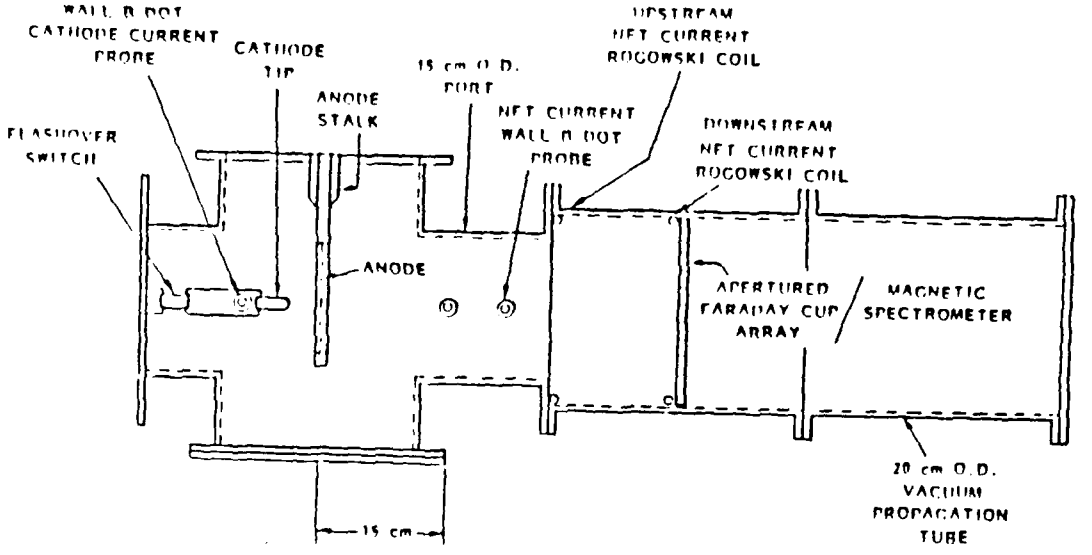

Fig. 6. Plasmoid experimental configuration.

4. RESULTS AND DISCUSSION

A 'foilless' ion diode configuration was usually employed. That is, rather than having a fixed ground screen electrode downstream of the anode, the near-zero potential within the drift tube was used to accelerate the ion (and decelerate the electrons). The cathode tip used was planar, 1.1 cm in diameter, and covered with velvet cloth to improve emission characteristics[5]. To achieve optimum simultaneity, the exact length of the flashover switch was varied depending on the anode voltage, A-K gap distance, and cathode size. When tuned, simultaneity was excellent, with cathode current turn-on occurring within 2 nsec of anode voltage.

One occasional problem which adversely affected the operation of the diode was the finite turn-on time of the anode. That is, space charge limited emission of ions from the anode cannot begin until formation of plasma. This process was found to take as long as 20 nsec, so that, although the voltages were produced simultaneously, the ion current did not flow until 20 ns. later. Evidence of the ion current delay was seen in the time-resolved impedance of the diode. Using the measured voltage and current as inputs, we found the ratio of diode current to Child-Langmuir electron current as a function of time early in the pulse for a single shot. Between about 12 nsec and 20 nsec the ratio changes from unity to approximately 1.9, indicating a shift from unipolar to bipolar flow, or the beginning of ion current.

The inferred proton and electron terminal velocities, from conservation of energy, are approximately .03c-.04c and .,2c-.5c, respectively. Note that at these low electron energies, the considerations presented in Section II would indicate that for radial equilibrium downstream, one would expect the ratio of ion to electron current to be just slightly less than the corresponding velocity ratio, and the required area ratio of the two beams to be approximately one.

The signals shown in Figure 7 also provide us with a check of ion energetics from the delay of net current with respect to diode current. In the figure, one can see the ion current turn on at approximately 20 nsec into the pulse. At this time, the anode voltage is about 520 kV, corresponding to an ion velocity of 1.0×10^7 m/sec. Thus, the ions should arrive at the 20 cm downstream position about 40 nsec after the

beginning of diode voltage and current. In Figure 7b, the net current is displayed on the same oscilloscope as the anode current, and one can see that the net current delay is, in fact, just about 40 nsec.

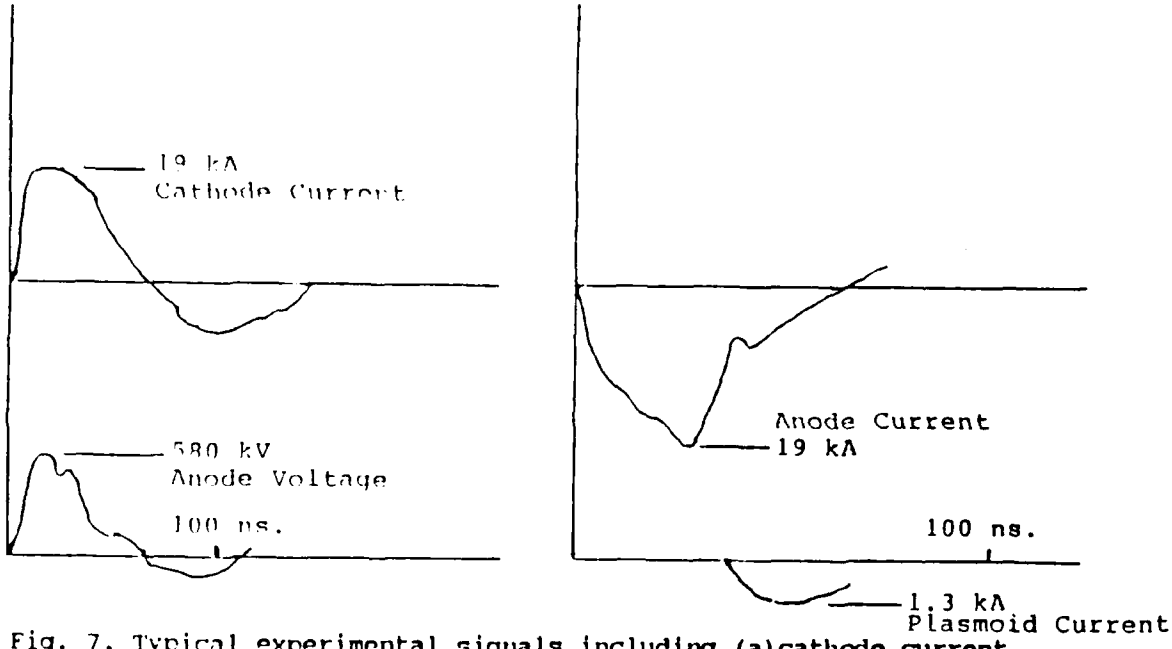

Fig. 7. Typical experimental signals including (a)cathode current and anode voltage, and (b)anode and net currents.

In general, inferred peak current densities on axis were approximately 10-15 A/cm2 for electrons and 1 A/cm for ions. These values are roughly consistent with estimates based on the velocity ratio.

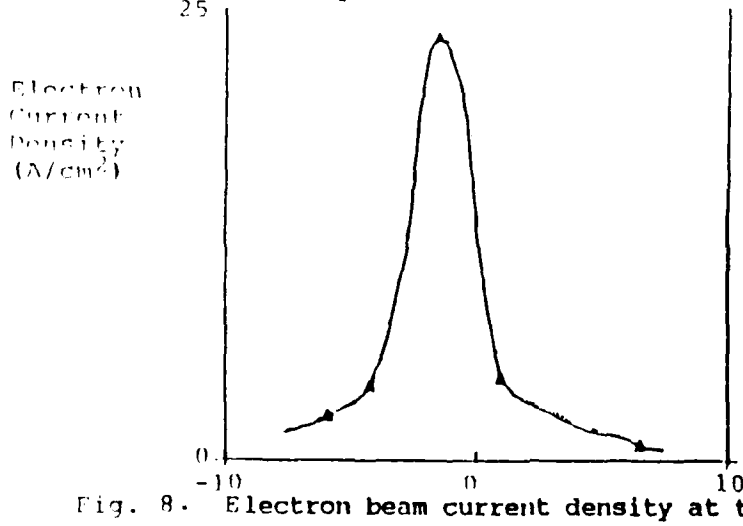

Fig. 8. Electron beam current density at the tube end.

In Figure 8 we have plotted the unfolded current density radial profiles for a particular shot. The inferred peak net current density is in agreement with the spectrometer data ignoring secondary electron contributions. Note also, that the profile is centrally peaked with a FWHM radius of a few centimeters. This type of profile was observed for almost all shots. In addition, an offset in the beam center was consistently seen--always in the same direction. Upon careful examination of the

setup, it was concluded that the displacement was due to the asymmetric anode feed.

To summarize, the Plasmoid diode behaves as anticipated, although in some cases ion current is delayed with respect to electron current. We believe this delay is due to finite anode plasma formation time, and is certainly a function of electron current density and voltage as well as physical details of the anode. The electron and ion beams generated in the diode are well above the space charge limited currents for either specie within the propagation tube and do not, in general, support a radial equilibrium. The entire assembly then propagates in a coherent manner at the ion axial velocity, with the faster electron emerging through the beam head continuously and rapidly leaving the system radially due to space charge repulsion. The beams thus propagating can be more than an order of magnitude greater in current than either electrons or ions individually.

ACKNOWLEDGEMENTS

The authors would like to thank M. Williams for his technical work on this experiment. This work was supported by the Air Force Office of Scientific Research under contract number F49620-85-C-0022.

REFERENCES

1. Present address, North Star Research Corp., Albuquerque, NM.

2. W.H. Bostick, Phys. Rev. Lett. 104, 292 (1956).

3. This configuration is similar to that presented in: R.J. Miller et. al., Phys. Fluids 24, 347 (1981). or W.W. Destler et. al., Phys. Fluids 27, 1897 (1984).

4. J.W. Poukey, Appl. Phys. Lett. 26, 145 (1975).

5. R.J. Miller et. al. Rev. Sci. Instrum. 56, 76 (1985).

END

DATE

FILMED

6-88

DTIC